ELSEVIER

Precambrian Research 104 (2000) 47–75

Precambrian Research

www.elsevier.com/locate/precamres

# Paleoproterozoic late-orogenic and anorogenic alkaline granitic magmatism from northeast Brazil

J. Plá Cid [a,*], M.F. Bitencourt [a], L.V.S. Nardi [a], H. Conceição [b], B. Bonin [c], J.M. Lafon [d]

[a] *Curso de Pós-Graduação em in Geociências, Campus de Agronomia, Instituto de Geociencias, University Federal do Rio Grande do Sul (UFRGS), Av. Bento Gonçalves, 9500, CEP-91509-900 Porto Alegre, RS, Brazil*

[b] *CPGG-PPPG/UFBA, Rua Caetano Moura, 123, Instituto de Geociências, UFBA, CEP-40210-350, Salvador, BA, Brazil*

[c] *Departement des Sciences de la Terre, Laboratoire de Pétrographie et Volcanologie, Université Paris, Sud. Centre d'Orsay, Bat. 504, F-91504 Paris, France*

[d] *Centro de Geociências, Laboratório de Geologia Isotópica, Universidade Federal do Pará (UFPA), Pará, Brazil*

Received 21 January 1999; accepted 4 May 2000

**Abstract**

During the Transamazonian cycle ($2.0 \pm 0.2$ Ga), two silica-saturated alkaline granite suites were intruded along the border of the São Francisco craton, northeastern Brazil. The Couro de Onça intrusive suite (COIS) is late tectonic relative to major deformational events, and the Serra do Meio suite (SMS) postdates this event, being interpreted as anorogenic type, deformed during the Brasiliano cycle (0.65–0.52 Ga). The COIS encompasses alkali-feldspar granites, syenogranites, monzogranites, with dykes of similar composition and age ($2.157 \pm 5$ Ma). They are metaluminous rocks of alkaline affinity, whose evolution was probably controlled by mineral fractionation processes involving mainly plagioclase, amphibole, and Fe–Ti oxide. The SMS, whose probable age is 2.01 Ga, is composed of metaluminous and peralkaline granites, with associated quartz syenites, with Ti-aegirine transformed during the Brasiliano deformation to riebeckite + titanite + aenigmatite. The temperatures of two stages of metamorphic transformation, overprinted during the Brasiliano event, are estimated at about 550 and 400–450°C. Both magmatic suites are derived from enriched mantle sources. The metaluminous and peralkaline trends observed in the SMS, characterized by high concentrations of HFS and RE elements controlled mainly by F-activity, reflect the evolution of different primary magmas produced by successive melting of the same mantle sources, in an anorogenic setting.


*Keywords:* Alkaline granites; Geochemistry; Anorogenic; Late-orogenic

## 1. Introduction

The studied region is situated near the border of the Bahia state, northeast Brazil (Fig. 1A). Two alkaline suites, which intrude Archean to

* Corresponding author.

*E-mail addresses:* placid@if.ufrgs.br (J. Plá Cid), lnardi@if.ufrgs.br (L.V.S. Nardi), herbet@pppg.ufba.br (H. Conceição), bbonin@geol.u-psud.fr (B. Bonin), lafonjm@ufpa.br (J.M. Lafon).

0301-9268/00/$ - see front matter 
PII: S0301-9268(00)00081-4

Paleoproterozoic sequences, have been investigated for their geological, petrographical, geochemical and geochronological aspects. The Couro de Onça intrusive suite (COIS) corresponds to the Couro de Onça granites, as proposed by Plá Cid et al. (1997a) to encompass four granitic bodies which intrude Archean TTG gneisses. The Serra do Meio suite (SMS) corresponds partly to the term previously employed by Leite (1997) with the exception of the peraluminous granites, as pointed out by Plá Cid (1994). Thus, the term refers to the granitic magmatism which is part of the Campo Alegre de Lourdes alkaline province (Conceição, 1990).

The SMS has been studied by Leite (1987), Conceição (1990), Plá Cid (1994), Leite (1997), who presented consistent petrographic, electron microprobe, and geochemical data. In this paper,

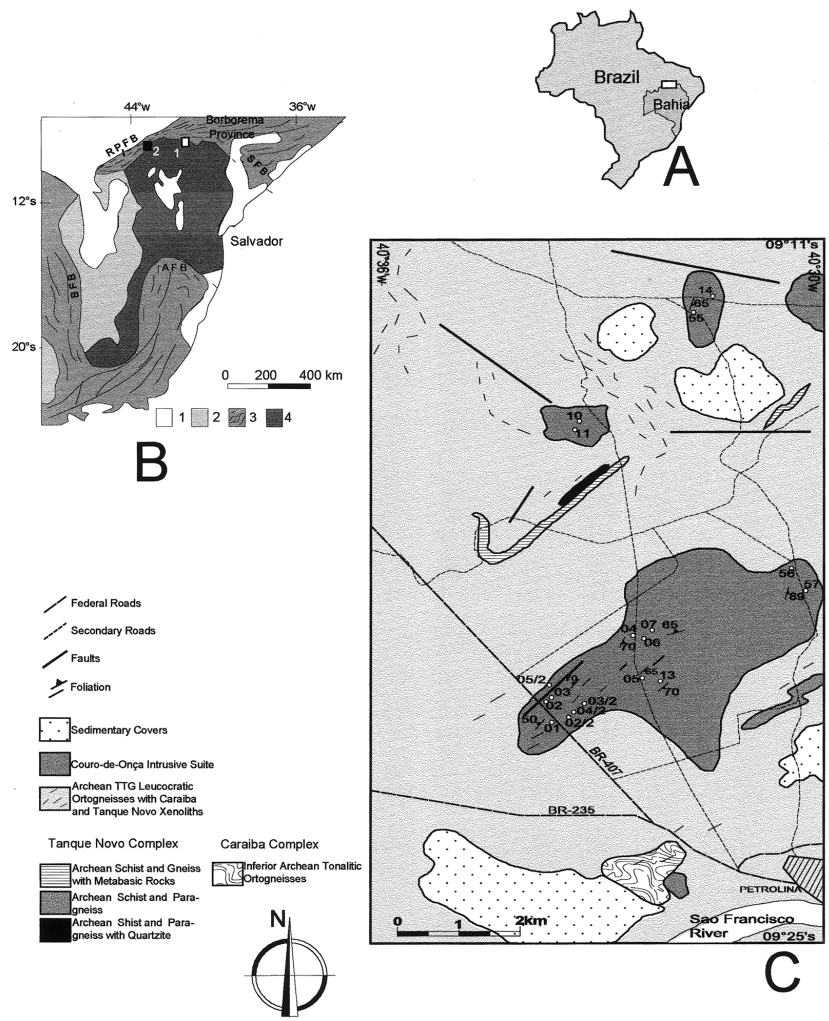


Fig. 1. Bahia state in northeast Brazil, with location of studied areas-A. Main geological units of the São Francisco Craton, after Almeida et al. (1977), 1, Phanerozoic cover; 2, Neoproterozoic cover; 3, Neoproterozoic fold belts, and 4, Craton terrains. Alkaline granites in rectangles. Brasiliano Riacho do Pontal and Rio Preto (RPFB); Araçuaí (AFB); Sergipano (SFB) and Brasília fold belts (BFB)-(C). Couro de Onça intrusive suite (1) and Serra do Meio suite (2)-B. Simplified geological map of the COIS, after Figuerôa and Silva Filho (1990) (modified). White circles indicate the visited outcrops-C.

additional petrographic data and new electron microprobe analyses are shown, as well as a re-interpretation of the geochemical data, with emphasis on magmatic derivation and possible sources. Isotopic determinations at Campo Alegre de Lourdes alkaline province point to emplacement related with the Transamazonian event ($2.0 \pm 0.2$ Ga, Wernick, 1981), as evidenced by U–Pb data from zircon/baddeleyite in the Angico dos Dias Carbonatite (2.01 Ga, Silva et al., 1988).

Field relations, geochemical and isotopic data of the COIS and other granitoids from this area were studied by Figuerôa and Silva Filho (1990). Geochronological data from high-K calc–alkaline granitoids indicate a Transamazonian magmatism (2.0 Ga) related to Paleoproterozoic transcurrent deformation. According to these authors, the COIS is probably late to post-strike-slif. Pb–Pb in zircon isotopic determinations, as well as field structures, petrographic and geochemical data from COIS, are presented and discussed in this paper, together with some electron microprobe analyses of amphibole and plagioclase.

## 2. Geological setting

The studied magmatic suites are intrusive in two main geotectonic units in northeast Brazil, the São Francisco craton (SFC), and the Riacho do Pontal fold belt (RPFB) (Fig. 1B). The RPFB, which represents the northwestern border of the cratonic terrain, is one of the several Brasiliano-age (0.65–0.52 Ga Van Schmus et al., 1995; Barbosa and Dominguez, 1996) fold belts surrounding the SFC. According to Brito Neves (1975), major ENE–WSW trending structures in the RPFB were developed during the Neoproterozoic. Jardim de Sá (1994) concluded that the Brasiliano cycle in most fold belts from northeast Brazil is characterized essentially by intracontinental reworking, showing no evidence of subduction-related settings. On the other hand, the same author, based on structural patterns, geochemical and geochronological data, suggested a Paleoproterozoic subduction setting in these terrains, which has promoted extensive mantle metasomatism. In fact, the geochemical patterns of Brasiliano-age ultrapotassic magmatism (Ferreira et al., 1994; Plá Cid, 1994), confirm a subduction signature, attributed to the Transamazonian (Paleoproterozoic) cycle.

The São Francisco craton (SFC) has been a stable crustal terrain since 0.52 Ga (Van Schmus et al., 1995), which corresponds to the last stages of the Brasiliano cycle. This cratonic structure is roughly represented by an Archean nuclei cross-cut by NS-trending Paleoproterozoic belts. Within these older nuclei, TTG associations, as well as charnockitic, enderbitic, and metasedimentary rocks of 2.6–3.3 Ga (Barbosa and Dominguez, 1996) are found. The Paleoproterozoic belts are characterized by widespread occurrence of syenitic and granitic rocks of alkaline, shoshonitic and ultrapotassic signatures (Conceição, 1990). The syenitic rocks are late-Transamazonian, about 2.0 Ga in age (Conceição, 1990, 1994; Rosa, 1994).

According to Leite et al. (1993), Plá Cid (1994), Leite (1997), the Brasiliano event in this area is responsible for the collision of crustal blocks, which has resulted in extensive thrust tectonics along ENE–WSW striking surfaces (Fig. 2). Transport direction along these planes is top-to-NW. NS-striking, km-wide transcurrent zones located to the east of thrust structures have been interpreted by Leite (1997) as lateral ramps, active during the same event. Ductile shearing structures found in the SMS granitoids are attributed to this event, and occur both along main thrust planes and lateral ramps.

A pre-Brasiliano, possibly Transamazonian, extensional setting is argued for this area (Plá Cid, 1994; Leite, 1997), which is succeeded by intensive sedimentation events during Mesoproterozoic times (Leite, 1997). Such tectonic framework is compatible with the assumption made by Plá Cid (1994) that lithological contacts in the SMS, as observed now, do not represent original igneous geometry, but result from strong superposition of tectonic events during the Brasiliano cycle.

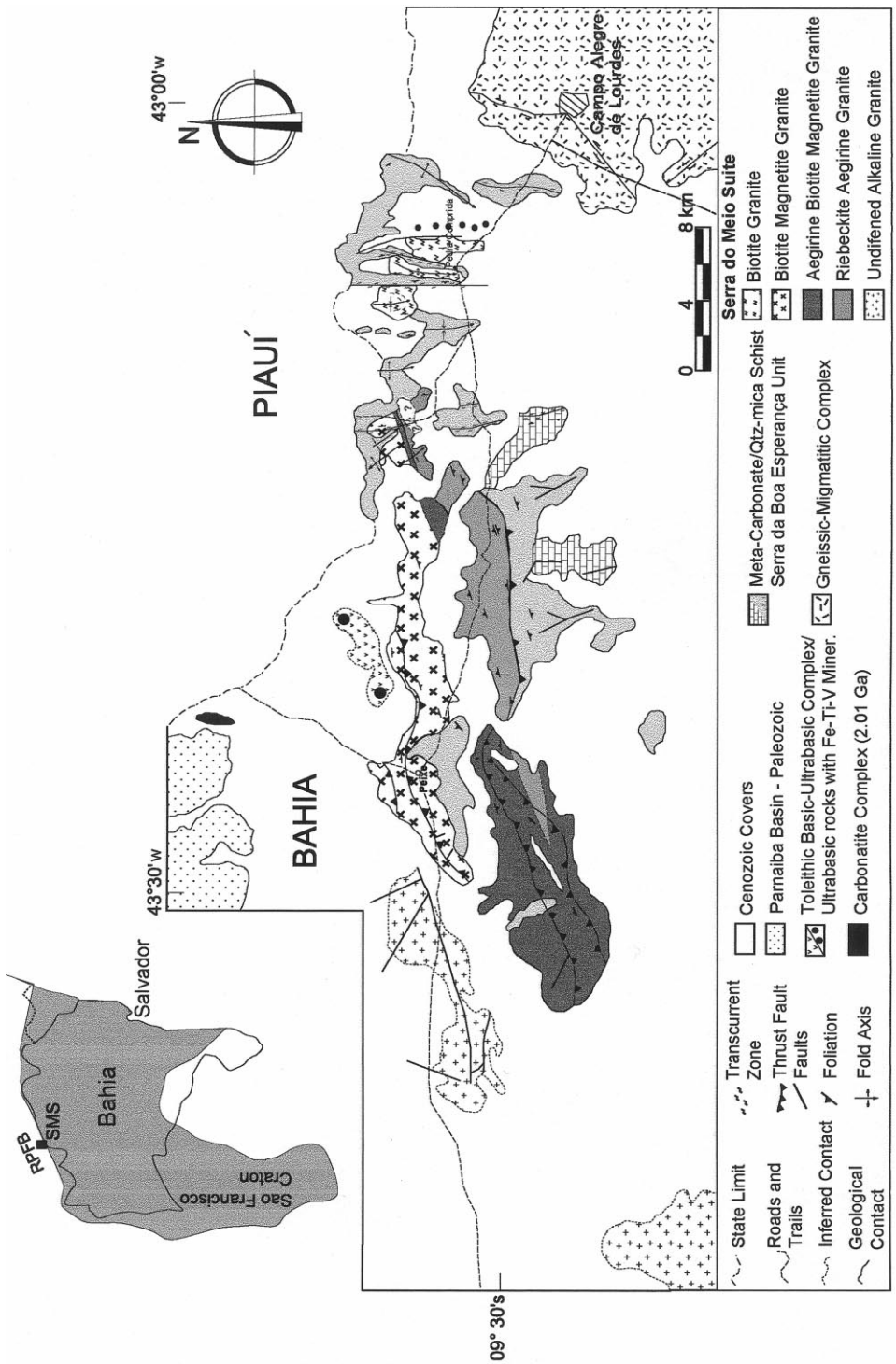


Fig. 2. Geological map of the Campo Alegre de Lourdes region, showing the SMS, after Leite (1997) (modified).

## 3. Local geology

The studied granitic suites are represented by, (i) SMS, part of the Campo Alegre de Lourdes Alkaline Province (Leite, 1987; Conceição, 1990; Plá Cid, 1994); and (ii) Couro-de-Onça Intrusive suite (COIS- Figuerôa and Silva Filho, 1990; Plá Cid et al., 1997a,b). These suites are intrusive in the cratonic rocks (COIS, Fig. 1B), next to the limit with RPFB, and within the fold belt terrains (SMS, Fig. 1b).

### *3.1. Serra do Meio suite*

This suite is intrusive in the RPFB terrains (Fig. 2), where Leite (1997) identified six different units, (i)-the gneissic–migmatitic complex, of Archean age, as indicated by a Rb–Sr determination of 2.6 Ga (Dalton de Souza et al., 1979), composed of two mica-bearing ortogneisses of granitic composition, migmatitic gneisses of trondhjemite–tonalite composition, and leucocratic gneisses of granitic composition. According to Dalton de Souza et al. (1979), this complex is metamorphosed in the amphibolite facies; (ii)-the Serra da Boa Esperança unit, encompassing metasedimentary rocks of greenschist facies, is composed of quartz-mica schist and calcareous schist, with inferred Paleo to Mesoproterozoic age; (iii)-the Santo Onofre group, composed of strongly recrystallized metapsamitic and metapelitic rocks of Mesoproterozoic age; (iv)-the plutonic rocks, comprising tholeiitic to transitional basalts (Couto, 1989), a carbonatitic complex, and alkaline granites (SMS), in addition to mafic and ultramafic plutons. The basaltic rocks are characterized by significant Fe–Ti-(V) deposits (Couto, 1989). The plutonic rocks were deformed and metamorphosed during the Brasiliano cycle, which confirms its pre-Brasiliano emplacement age (Couto, 1989; Plá Cid, 1994). Whole-rock Rb–Sr determinations show that these granites have undergone strong isotopic system opening, with ages varying from 500 to 850 Ma, which represent a mixing age between the end of Brasiliano cycle and crystallization age (Plá Cid, 1994), (v)-the Parnaíba basin, formed by sedimentary rocks with late-Ordovician to early-Carboniferous age, and (vi)-Cenozoic cover sediments.

The SMS constitutes several intrusions of ca 400 km$^2$ total area within a major ENE–WSW alignment (Fig. 2). They intrude the Paleoproterozoic Serra da Boa Esperança unit (Silva et al., 1988; Leite and Fróes, 1989; Leite et al., 1993), as well as the Archean gneissic–migmatitic complex. cm To m-sized xenoliths of the former unit are abundant within these intrusions. Granites have gneissic, locally mylonitic structure, with a marked foliation, attributed to the Brasiliano collisional cycle (Jardim de Sá, 1994), trending ENE–WSW (Fig. 2) and dipping less than 25° towards SE or NW. In the northeastern portion of this granitic belt, NS-trending transcurrent zones are dominant, and imprint on the granites a foliation which dips at an angle usually higher than 45°.

The alkaline granites are leucocratic, with fine-grained and inequigranular texture marked by alkali-feldspar phenocrysts, as well as riebeckite and magnetite porphyroblasts. The gneissic structure evolves locally into a mylonitic one (Plá Cid, 1994), although in some outcrops the granites show pod-like portions of coarse-grained and isotropic rocks, surrounded by deformed portions. In spite of the Brasiliano-age deformation in this area, the alkaline granites sometimes preserve igneous structures, such as biotitic schlieren, found near the village of Peixe (Fig. 2), as well as coarse-grained, isotropic textures, as previously described. Enclaves (autoliths) and dykes are not observed.

Alkaline granites are not commonly deformed. However, deformational features are described in alkaline suites of similar tectonic environment, such as the Willyama supergroup, Olary Block (South Australia, Ashley et al., 1996) and Nogoya granites (South Africa, Scogings, 1986).

### *3.2. Couro-de-Onça intrusive suite*

These intrusions are located in the northwestern border of the SFC (Fig. 1), near the town of Petrolina (Fig. 1C). The following Archean units have been identified by Figuerôa and Silva Filho (1990) in this portion of the SFC, (i) the Caraíba complex, formed by gneisses and migmatitic ortogneisses, both with trondhjemite–tonalite–gra-

nodiorite composition; (ii) volcano-sedimentary sequences, represented by the Rio Salitre and Tanque Novo complexes, the former including schists, paragneisses, quartzites, and banded iron-formations, and the latter containing mafic-ultramafic and felsic volcanic rocks. (iii) Archean gneisses to orthogneisses of TTG composition which are intrusive in these metamorphic complexes, as suggested by the presence of xenoliths of the Rio Salitre and Tanque Novo rocks.

The magmatic rocks are represented by syn- to late-tectonic granites, relaated to the Transamazonian cycle, represented by, (a) Sobrado-type granitoids of calc–alkaline affinity (Figuerôa and Silva Filho, 1990), where Rb–Sr isotopic determinations indicate an age of $2004 \pm 107$ Ma, and $Sr_i$ ratio of 0.737; (b) biotite monzogranites of alkaline affinity and age of $1928 \pm 409$ Ma, obtained by Rb–Sr isotopic method (Figuerôa and Silva Filho, 1990) and, (c) COIS, with isotopic data obtained by Pb–Pb in zircon suggesting crystallization age of $2157 \pm 5$ Ma (Plá Cid, 1994). Seven crystals were analyzed, and the obtained age varies from 2142 Ma, considering three grains, to 2157 Ma, four grains. The data confirm the late-Transamazonian age of this intrusive suite.

The COIS is composed of at least four plutons of irregular to slightly circular shape, comprising a total area of about 35 $km^2$ (Fig. 1C). These granites are intrusive in Archean trondhjemite–tonalite–granodiorite rocks (Figuerôa and Silva Filho, 1990), found as centimeter to meter-sized xenoliths. The rocks are medium-grained, leuco- to mesocratic, medium-gray or pink in color, and have a pronounced foliation, marked by the alignment of amphibole crystals. Banded (gneissic) structure is sometimes observed, parallel to the main foliation. Massive structure is locally present. The dominant orientation trends 010–050°, dipping 45–70° NW, locally to SE. Centimeter-sized shear zones are parallel to the granite foliation, and imprint a locally mylonitic structure on these granites, suggestive of their syn- to late-tectonic emplacement. Mafic minerals occur in two principal forms, (i) irregular to circular clots containing amphibole and biotite of medium grainsize, and (ii) smaller-sized, widespread amphibole crystals.

The banding is characterized by alternating, 10–15 cm thick bands of mesocratic and leucocratic granitic compositions. Near to outcrops 12 and 13 (Fig. 1C), the COIS foliation is folded, with axial planes parallel to the banded structure. m-Sized xenoliths of gneissic basement rocks are also found here, which are partially assimilated by the host granites.

A common feature is the presence of synplutonic-dyke swarms, either with coarse-gained or pegmatitic texture, the latter ones showing dm-sized lenses of blue quartz. Both have centimetric to metric thickness, and display diffuse contacts with granitic host rock. Two preferential orientations have been observed for these dykes, an earlier one, striking 080°, and dipping 60° towards NW, represented by coarse-grained dykes, and a later one, which crosscuts the former, trending 025° and dipping 30° NW, represented by coarse-grained and pegmatitic types.

Their composition varies from alkali-feldspar granites to monzogranites, both having amphibole as the dominant mafic phase. Pegmatitic dykes are of subordinate occurrence and contain blue-quartz, alkali-feldspar and amphibole. Commonly, one of the contacts between dyke and granitic host rock is irregular and diffuse, while the other is sharp. The sharp, upper contact is also marked by coarsening of minerals in the dyke, which shows progressive grainsize decrease towards the lower, diffuse contact. The orientation of mafic minerals within folded dykes is similar to the one in the host rocks. These characteristics are suggestive of the synplutonic character of these dykes. The occurrence of coarser grainsize at the upper contact is probably related to an original volatile gradient established during emplacement.

Local assimilation of dyke rocks by the granites is also observed. Near these intrusions, a number of fragments are found within the host rock, which shows progressive textural modification due to partial assimilation processes. The coarser margins, containing amphibole-plagioclase concentrations, remain virtually intact.

## 4. Petrographic features

### 4.1. Serra do Meio suite

These rocks are alkali-feldspar granites, with subordinate quartz–alkali-feldspar syenites, showing strong mineral alignment and recrystallization features. In spite of their strong solid-state deformation, probably of Brasiliano age, original magmatic minerals, such as alkali-feldspar phenocrysts and some mafic phases, are preserved. The SMS granites are formed by alkali-feldspar, quartz, albite, microcline, aegirine, aegirine–augite, hedenbergite, riebeckite, magnetite and biotite. Accessory minerals are titanite, allanite, aenigmatite, fluorite, apatite and zircon, and calcite occurs as a secondary mineral phase.

Three different facies were identified. Metaluminous types, with biotite as the only mafic mineral, slightly peralkaline granites with aegirine crystals, and strongly peralkaline ones, presenting riebeckite–aegirine–aenigmatite paragenesis. The main petrographic evidence for preserved igneous textures, as well as metamorphic assemblages, are shown in the Tables 1 and 2. Specific features of each type are discussed below.

#### 4.1.1. Metaluminous granites

These are alkali-feldspar granites with interstitial, subhedral, brown to greenish-brown biotite. The foliation is marked by alignment of interstitial crystals, and also by elongate, millimetric, biotite concentrations. Colorless and purple fluorite grains are interstitial. In the northeastern plutons, these characteristics are dominant, but in the central portion of the belt (Fig. 2), biotite is sometimes transformed into muscovite, associated to magnetite blasts and interstitial calcite, suggesting the presence of Fe–$CO_2$-rich fluids. Microprobe data indicate that these are annitic biotites (Conceição, 1990; Plá Cid, 1994; Plá Cid et al., 1995).

#### 4.1.2. Slightly peralkaline granites

These are represented by alkali-feldspar granites, which predominate over quartz–alkali-feldspar syenites. The mafic mineralogy is composed of green and colorless pyroxene, biotite and occasionally magnetite. The green to pale-green crystals are aegirine (Ac 72–94%), and aegirine–augite (Ac 60–72%); colorless pyroxene was optically identified as hedenbergite. Hedenbergite and aegirine–augite grains are interpreted as magmatic mafic minerals, since metamorphic temperature estimations, as discussed later, are below their stability field. Acicular, greenish crystals are included in the cores of alkali-feldspar phenocrysts, not observed in the newly-formed, clear borders, attesting their magmatic origin. Sometimes, as shown by Conceição (1990), Leite et al. (1991), these included crystals are aegirine–augite in composition. Aegirine constitutes either phenocryst, enclosing alkali-feldspar, albite, and quartz, or randomly distributed, interstitial crystals.

#### 4.1.3. Strongly peralkaline granites

These are represented by alkali-feldspar granites, with local occurrence of the quartz–alkali-feldspar syenites, showing strong variation of mafic mineral contents, which are riebeckite, aegirine, aegirine–augite, colorless pyroxene, aenigmatite, biotite, and magnetite. The strongly peralkaline granites exhibit preserved original magmatic textures, such as zoned, subhedral crystals of mafic minerals, and magmatic mafic minerals included in alkali-feldspars. The amphibole was identified as riebeckite (Conceição, 1990; Plá Cid, 1994), constituting dark-blue to brownish-blue poikilitic phenoblasts, and interstitial subhedral grains. Leite et al. (1991) argues for two different generations of riebeckite. The interstitial crystals, recrystallized during the tectonic deformation and surrounded by aegirine, are parallel to the rock foliation, while the phenoblasts are not oriented, generated by recrystallization during late or post-tectonic stages. Poikilitic riebeckite encloses remnants of aegirine, as well as alkali-feldspar, quartz and albite. It is associated intimately with reddish, fibrous aenigmatite and euhedral titanite crystals on the borders. Riebeckite–aenigmatite–titanite association is assumed to be the latest mafic minerals to recrystallize.

Subhedral, zoned pyroxene phenocrysts are also present, which are crosscut by the foliation. They are interpreted as preserved magmatic pyroxene,

Table 1
Textural and mineralogical features of the Couro de Onça intrusive suite[a]

| | Quartz | Alkali-feldsper | Oligoclase | Browa amphibole | Blue amphibole | Biotite |
|---|---|---|---|---|---|---|
| Euhedralism | Generally anhedral; subhedral when included in feldspar | Subhedral to anhedral | Subhedral to anhedral | Subhedral to anhedral | Acicular and prismatic | Subhedral |
| Composition | – | – | An < 13% | Edenite | Hastingsite | Annite |
| Occurrence | – | – | – | Clots and disperse in the granites | Clots | Clots |
| Characteristics | Wavy extinction common in the foliated granites | Perthitic, with exsolved albite in internal borders, and albite–pericline twin, slight wavy extinction | Albite and albite-Carlsbad twinned; borders are locally corroded, with epidote growth in the core | Poiquilitic crystals, with zoning to blue amphibole in clots | In clots, acicular and euhedral prismatic grains | Brown to brown greenish color, commonly substituting amphiboles |
| Orientation | Frequently elongated (anhedral grains), with subgrains in the borders | Frequently, flame-type perthites, parallel to the foliation | Not necessarily oriented | Poiquilitic grains are frequently oriented | Not oriented | Not oriented |
| Textural relations | In clots presents subgrains and the contacts are straight, with polygonal texture | Internal rims of exsolved albite in alkali feldspar, in contact with pre subsolvus quartz | Irregular milimetric needles, sometimes interstitial to alkali-feldspar and quartz; spongy cellular texture suggest partial resorption (Hibbard, 1995) | Partial substitution by biotite at the borders and along the cleavages; common as relicts in biotite and blue amphibole within clots | The closts are surrounded or associated with microgranular concentrations of blue amphibole, quartz and biotite | Sometimes part of the clots, with titanite, oxide and euhedral epidote, with brown amphibole relicts; associated to zircon, allanite and apatite |
| Contact relations | With feldspars are frequently sinuous | With oligoclase and quartz are irregular and sinuous | With alkali-feldspar and quartz are irregular and sinuous; mutual embayment | Frequently straight | Frequently straight | Frequently straight |
| Inclusions | In the elongated grains, alkali-feldspar, oligoclase and brown amphibole; apatite in foliated terms and zircon in massive ones | Oligoclase relicts and quartz rounded, zircon and brown amphibole grains; apatite-oriented terms; allanite-isotropic ones | Acicular blue amphibole and euhedral biotite close to the clots | Quartz, alkali-feldspar and oligoclase; apatite and zircon grains are common inclusions | Not observed | Amphibole relicts |

[a] The mineral compositions were obtained by electron microprobe.

Table 2
Summary of the main igneous and metamorphic features observed in the Serra do Meio suite[a]

| | Igneous texture | High temperature metamorphic features | Low temperature metamorphic features |
|---|---|---|---|
| Alkali-feldspar | Perthitic (in veins) phenocryst cores preserved | Patch-perthite; sometimes with sub-grains | Alkali-feldspar clear borders surrounding phenocrysts |
| Quartz | | Quartz 'ribbons' | Polygonal texture (annealing), sometimes with alibite and microcline granoblastic texture |
| Microcline + albite | | Newly-formed grains, with secondary twin | Granoblastic texture |
| Mafic minerals | Ti-bearing aegirine zoned phenocrysts; micro-inclusions of aegirine and aegirine–augite in alkali-feldspar; subhedral zoned mafic grains, enclosed in alkali-feldspar, with arfvedsonitic cores | First generation of riebeckite, interstitial and oriented along foliation; this type is surrounded by aegirine, which can occur as individualized grains along foliation; biotite orientation | Second generation of riebeckite, constituted by porphyroblastic grains of random orientation; transformation of these crystals to aenigmatite + titanite |
| Interpretations and temperature estimation | Hipersolvus conditions during alkali-feldspar crystallization; aegirine–augite and arfvedsonite minerals indicating crystallization temperatures of at least 700°C | Quartz ribbons, secondary twin in feldspars point to a ductile character of this deformational event (Hibbard, 1995); estimate temperature to this stage around 550°C | Annealing of quartz grains is an evidence of recrystallization in a static environment (Hibbard, 1995); temperature estimations between 400 and 450°C |

[a] More details are described in the text.

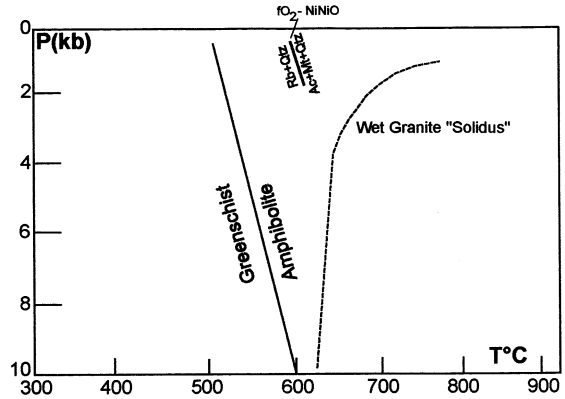


Fig. 3. Pressure (kb) vs. temperature (°C) diagram, showing the limit between greenschist and amphibolite metamorphic facies, and solidus curve of wet granite (Winkler, 1979). Subsolidus reaction of riebeckite + quartz↔aegirine + magnetite + Quartz (Ernst, 1962) is suggested as the upper limit of metamorphism in the SMS.

and microprobe data indicate Ti-aegirine and Ti-aegirine–augite composition for the dark-blue core zones, with titanium decreasing towards the dark-green borders. Thus, original, magmatic Ti-pyroxene, which has reacted during the Brasiliano-age deformation would result in a late-tectonic secondary mineral assemblage, constituted by riebeckite + titanite + aenigmatite.

Annitic biotite is subhedral, reddish-brown in colour, and occurs usually at the borders of alkaline minerals (Conceição, 1990; Plá Cid, 1994). Occasionally, dark amphibole included in alkali-feldspar and surrounded by aegirine–augite, presents riebeckite–arfvedsonite mixed composition, which suggests a magmatic origin. Euhedral magnetite blasts can be observed along the foliation, suggesting high $fO_2$ conditions during the deformational event, due to Fe-rich fluids, as previously described. Subhedral and anhedral, interstitial fluorite is a common accessory phase, associated with the sodic mafic minerals.

Fig. 3 shows the boundary between greenschist–amphibolite metamorphic facies conditions, the wet granite solidus, and the stability field for riebeckite, which reacts with quartz + fluid and is transformed into aegirine + magnetite + quartz + fluid. This reaction, occurring under amphibolite conditions, is the upper limit of metamorphism for the alkaline granites. As shown in Table 2, riebeckite grains surrounded by aegirine are common syntectonic features. The reaction observed in Fig. 3 indicates that the paragenesis present in the granites is compatible with a progressive metamorphic origin, in temperature slightly below 600°C. Temperatures below 600°C are assumed to be the strongest register of metamorphism in the SMS. At such temperatures, Brasiliano-age metamorphism has affected the subsolidus minerals, and igneous features are partially preserved.

### 4.2. *Couro-de-Onça intrusive suite*

These rocks comprise alkali-feldspar granites to syenogranites, with subordinate monzogranites. The associated dykes have similar compositions. Quartz-monzodioritic rocks are only found as relicts of partially digested dyke material, as seen in outcrops 01 and 12 (Fig. 3). Isotropic rocks generally correspond to more evolved petrographic types, as syenogranites or alkali-feldspar granites. The foliated rocks are richer in plagioclase, ranging from syenogranites to monzogranites. The main petrographic features of these granites are summarized in Table 1.

The Couro-de-Onça granites are medium to coarse, locally fine-grained, inequigranular rocks. Alkali-feldspar and quartz grains may reach up to 3.0 mm, and occasionally, brown amphibole and oligoclase occur up to 2.0 mm. The groundmass is constituted by medium-grained alkali-feldspar, oligoclase, quartz, albite, brown and blue amphibole, biotite, opaque minerals and titanite. Zircon, apatite, allanite, and epidote are accessory phases. Alotriomorphic to hypidiomorphic texture is characteristic, and sinuous contacts are common, mainly between quartz and feldspars, with embayment of quartz grains. The orientation is marked by poikilitic, brown amphibole and mesoperthitic alkali-feldspar, with exsolved lamellae being parallel to the foliation. Occasionally, amphibole is concentrated in millimeter-thick, irregular levels. The dykes are coarse grained to pegmatitic, and alkali feldspar–quartz–oligoclase exhibit glomeroporphyritic texture.

Mafic clots, with ca. 2.0-mm diameter, are widespread. They are composed of quartz in the central region, surrounded by acicular, prismatic, blue amphibole, and euhedral biotite. Remnants of brown amphibole are found within blue-amphibole grains. Blue amphibole, biotite, and felsic minerals frequently show microgranular texture in the outer portions of these clots. Euhedral allanite, subhedral zircon and apatite, as well as euhedral oxide minerals, are accessory phases. Biotite is sometimes intergrown with mesoperthitic alkali-feldspar.

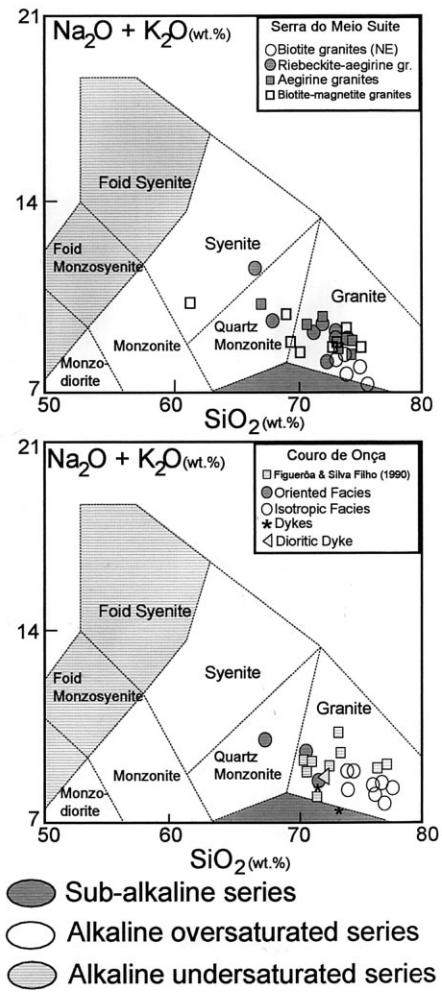


Fig. 4. Total alkalis vs. silica (TAS) diagram, after Le Maitre et al. (1989), with chemical classification and nomenclature of plutonic rocks according to Middlemost (1994). Magmatic series after Le Maitre et al. (1989).

Textural relations, such as plagioclase partial resorption, blue-amphibole acicular inclusions in oligoclase, microgranular agglomerations, and reverse zoning in amphibole are evidence that a simple magmatic history is not observed for these granites. In order to understand these features, it is necessary to remember that the magmatic system has been disturbed by synchronic intrusion of dykes having similar geochemical features. Thus, even if these dykes have not caused modification of geochemical signature, it is probable that the decompression undergone by the crystallizing granitic magma at the time the dykes were emplaced, as well as the fluid circulation promoted by coarse to pegmatitic dykes intrusion, have induced some changes in $P_{fluids}$ and total $P$ of the granite host. Microgranular textures, in association with large grainsize of the clots, would attest to a heterogeneous distribution of $P_{fluids}$. Some compositional change in amphibole may also be related to a new $F^-$, $H_2O$ or $Cl^-$ contents founds in magma.

## 5. Geochemistry

Whole-rock chemical analyses were obtained at the laboratories of Centro de Estudos em Petrologia e Geoquímica, Universidade Federal do Rio Grande do Sul, Brazil, Activation Laboratories Ltd., Ont., Canada, and Centre de Recherches Pétrographiques et Géochimiques (CRPG), Nancy, France. For the Couro-de-Onça granites, the analytical data of Figuerôa and Silva Filho (1990) were used. Analytical results are presented in Tables 3 and 4.

Both granitic suites are characterized by high alkali contents, confirming their alkaline signature. The COIS exhibits composition ranging from quartz-monzonite to granite, whereas dominant granitic composition is present in the SMS, with subordinate syenite and quartz-monzonite (Fig. 4). The COIS has dominantly metaluminous character, with slightly peralkaline and peraluminous compositions less common (Fig. 5). The Serra do Meio granites are essentially metaluminous and peralkaline, with riebeckite-bearing

Table 3
Whole-rock analyes of the Serra do Meio suite

| Sample<br>Facies | CL-74<br>slight peralk | CL-87<br>slight peralk | GA-68<br>slight peralk | JP-49<br>slight peralk | JP-50<br>slight peralk | PPB-14<br>slight peralk | PPB-14a<br>met granite | CL-77<br>met granite | CL-88<br>met granite | GA-13<br>met granite | GA-14<br>met granite | GA-14b<br>met granite | PPB-28a<br>met granite | PPB-63<br>met granite | PPB-64<br>met granite | CL-090<br>met granite |
|---|---|---|---|---|---|---|---|---|---|---|---|---|---|---|---|---|
| $SiO_2$ | 72 | 73.2 | 74.5 | 67.3 | 74.5 | 70.7 | 69.3 | 72.9 | 75.1 | 74.1 | 70.2 | 69.5 | 73.9 | 61.5 | 73.2 | 71.7 |
| $TiO_2$ | 0.21 | 0.37 | 0.15 | 0.44 | 0.22 | 0.43 | 0.22 | 0.53 | 0.1 | 0.38 | 0.58 | 0.51 | 0.16 | 0.4 | 0.23 | 0.23 |
| $Al_2O_3$ | 12.4 | 11 | 12.1 | 13.4 | 11.8 | 12 | 13.5 | 12 | 12.1 | 10.8 | 12.2 | 13.2 | 12.4 | 14.4 | 13.4 | 13.2 |
| $Fe_2O_3$ | 2.3 | 3.7 | 0.64 | 4.3 | 1.4 | 4.2 | 3.1 | 3.2 | 0.58 | 3.8 | 1.9 | 2.2 | 0.92 | 7.5 | 1.5 | 0.37 |
| FeO | 1.8 | 1.5 | 1.8 | 1.8 | 2.2 | 1.5 | 1.68 | 1.7 | 1.4 | 1.8 | 3.5 | 3.2 | 1.7 | 1.7 | 1.5 | 3.2 |
| MgO | 0.1 | 0.12 | 0.1 | 0.14 | 0.21 | 0.13 | 0.1 | 0.17 | 0.1 | 0.2 | 0.32 | 0.12 | 0.1 | 0.32 | 0.19 | 0.1 |
| CaO | 0.65 | 0.45 | 0.79 | 1.3 | 0.57 | 0.77 | 0.92 | 0.07 | 0.67 | 0.38 | 1.2 | 1.1 | 0.72 | 1.6 | 0.42 | 0.76 |
| $Na_2O$ | 4.5 | 3.9 | 3.8 | 5.1 | 3.4 | 4.4 | 4.8 | 1.8 | 3.7 | 2.6 | 4 | 4.7 | 3.6 | 6 | 3.7 | 4.2 |
| $K_2O$ | 5.1 | 4.6 | 5 | 5.1 | 4.9 | 5 | 5 | 6.7 | 4.9 | 4.9 | 4.4 | 4.1 | 5.6 | 4.2 | 5 | 5 |
| MnO | 0.14 | 0.21 | 0.06 | 0.16 | 0.07 | 0.18 | 0.09 | 0.1 | 0.05 | 0.05 | 0.22 | 0.19 | 0.04 | 0.43 | 0.08 | 0.13 |
| $P_2O_5$ | 0.05 | 0.05 | 0.05 | 0.05 | 0.05 | 0.05 | 0.05 | 0.05 | 0.05 | 0.05 | 0.06 | 0.05 | 0.05 | 0.05 | 0.05 | 0.05 |
| $H_2Op$ | 0.28 | 0.23 | 0.35 | 0.11 | 0.33 | 0.11 | 0.39 | 0.5 | 0.42 | 0.54 | 0.25 | 0.28 | 0.35 | 0.39 | 0.22 | 0.17 |
| $CO_2$ | 0.28 | 0.43 | 0.48 | 0.64 | 0.19 | 0.24 | 0.63 | 0.11 | 0.41 | 0.08 | 0.77 | 0.73 | 0.18 | 1.1 | 0.19 | 0.5 |
| Total | 99.81 | 99.76 | 99.82 | 99.84 | 99.84 | 99.71 | 99.78 | 99.83 | 99.58 | 99.68 | 99.6 | 99.88 | 99.72 | 99.59 | 99.68 | 99.61 |
| F | 2100 | 930 | 1800 | 2300 | 2300 | 620 | 300 | 860 | 3900 | 2300 | 1800 | 640 | 3100 | 4100 | 2400 | 1800 |
| Cl | 20 | 20 | 20 | 20 | 20 | 23 | 20 | 20 | 20 | 20 | 20 | 20 | 20 | 20 | 20 | 44 |
| Agpaitic index | 1.04 | 1.04 | 0.96 | 1.04 | 0.92 | 1.05 | 0.99 | 0.85 | 0.94 | 0.89 | 0.93 | 0.92 | 0.97 | 1 | 0.86 | 0.93 |
| FeOt | 3.87 | 4.83 | 2.38 | 5.67 | 3.46 | 5.28 | 4.47 | 4.58 | 1.92 | 5.22 | 5.21 | 5.18 | 2.53 | 8.45 | 2.85 | 3.53 |
| Ba | 77 | 240 | 160 | 710 | 180 | 260 | 190 | 610 | 220 | 300 | 990 | 1310 | 140 | 190 | 220 | 330 |
| Nb | 150 | 200 | 120 | 190 | 130 | 130 | 210 | 110 | 140 | 170 | 120 | 75 | 120 | 230 | 160 | 120 |
| Cs | 5 | 5 | 5 | 5 | 5 | 5 | 8 | 5 | 5 | 5 | 8 | 5 | 5 | 5 | 5 | 5 |
| Rb | 150 | 130 | 190 | 150 | 160 | 120 | 76 | 200 | 280 | 160 | 120 | 81 | 210 | 120 | 160 | 130 |
| Hf | 28 | 34 | 10 | 21 | 12 | 23 | 35 | 16 | 8 | 22 | 8 | 26 | 12 | 25 | 15 | 15 |
| Sr | 17 | 36 | 35 | 140 | 39 | 30 | 74 | 33 | 42 | 25 | 120 | 120 | 43 | 26 | 35 | 40 |
| Y | 170 | 160 | 170 | 110 | 98 | 92 | 180 | 98 | 200 | 180 | 79 | 95 | 170 | 110 | 130 | 170 |
| Zr | 1160 | 1440 | 430 | 810 | 660 | 910 | 1300 | 690 | 260 | 1050 | 400 | 1200 | 460 | 960 | 790 | 600 |
| Ga | 53 | 33 | 46 | 41 | 33 | 38 | 41 | 29 | 44 | 36 | 33 | 36 | 41 | 38 | 38 | 40 |
| V | 8 | 8 | 5 | 8 | 8 | 8 | 8 | 11 | 8 | 8 | 14 | 8 | 8 | 8 | 8 | 8 |
| Th | 19 | 27 | 27 | 22 | 20 | 8 | 18 | 8 | 77 | 19 | 5 | 12 | 26 | 22 | 28 | 12 |
| U | 10 | 10 | 10 | 10 | 10 | 10 | 10 | 10 | 10 | 10 | 10 | 10 | 10 | 10 | 10 | 10 |
| Ta | 6 | 11 | 10 | 13 | 9 | 7 | 12 | 7 | 12 | 14 | 7 | 5 | 5 | 9 | 10 | 5 |
| Cu | 11 | 19 | 22 | 15 | 11 | 15 | 11 | 11 | 11 | 7 | 11 | 15 | 15 | 15 | 15 | 15 |
| Co | 23 | 51 | 28 | 51 | 45 | 23 | 34 | 45 | 34 | 28 | 45 | 34 | 39 | 51 | 45 | 34 |
| Ni | 59 | 18 | 59 | 29 | 12 | 24 | 18 | 24 | 29 | 24 | 41 | 18 | 24 | 18 | 18 | 29 |
| Cr | 116 | 52 | 116 | 52 | 39 | 39 | 52 | 52 | 39 | 52 | 77 | 26 | 26 | 52 | 26 | 77 |
| La | | 208.2 | | 155.1 | 100.1 | | | 111.6 | 50.13 | 166.7 | 70.87 | | 145.5 | 224.6 | 114.4 | 132.5 |
| Ce | | 436.6 | | 335.2 | 215.1 | | | 213.8 | 114.8 | 373.6 | 161.7 | | 303.2 | 474.7 | 244.4 | 305.3 |
| Nd | | 179.1 | | 144.4 | 93.82 | | | 105.9 | 56 | 170.2 | 76.78 | | 130.2 | 189.2 | 99.39 | 129.6 |
| Sm | | 29.26 | | 24.32 | 17.14 | | | 18.84 | 13.26 | 30.68 | 14.63 | | 24.39 | 30.79 | 18.05 | 23.65 |
| Eu | | 3.22 | | 2.61 | 1.31 | | | 2.579 | 0.56 | 3.96 | 2.34 | | 0.95 | 3.27 | 1.34 | 1.47 |
| Gd | | 20.39 | | 18.26 | 13.82 | | | 13.82 | 13.04 | 25.98 | 10.46 | | 19.72 | 20.16 | 14.33 | 18.48 |
| Dy | | 16.89 | | 16.23 | 12.95 | | | 10.72 | 16.2 | 22.34 | 7.86 | | 18.21 | 15.74 | 13.15 | 17.3 |
| Ho | | 3.18 | | 3.18 | 2.51 | | | 1.985 | 3.36 | 4.13 | 1.85 | | 3.51 | 2.97 | 2.49 | 3.34 |
| Er | | 7.6 | | 8.2 | 6.34 | | | 4.551 | 9.68 | 9.45 | 3.36 | | 8.79 | 7.11 | 6.03 | 8.36 |
| Yb | | 5.15 | | 7.04 | 4.78 | | | 3.217 | 8.12 | 6.42 | 2.34 | | 7.12 | 5.22 | 4.42 | 6.41 |
| Lu | | 0.62 | | 0.87 | 0.62 | | | 0.404 | 0.92 | 0.82 | 0.32 | | 0.87 | 0.65 | 0.53 | 0.77 |
| ΣRare earth elements | | 910.21 | | 715.41 | 468.49 | | | 487.42 | 286.07 | 814.28 | 352.51 | | 662.46 | 974.41 | 518.53 | 647.18 |

Table 3 (*Continued*)

| Sample facies | CL-05b NE met | CL-105 NE met | CL-54 NE met | CL-55 NE met | GA-13 NE met | CL-16 strong peralk | GA-14c strong peralk | GA-34 strong peralk | GA-39 strong peralk | GA-46 strong peralk | GA-46a strong peralk | TR-72 strong peralk | PPB-78a strong peralk |
|---|---|---|---|---|---|---|---|---|---|---|---|---|---|
| $SiO_2$ | 75.1 | 74 | 75.7 | 73.3 | 74.1 | 68.3 | 73.3 | 74.2 | 66.9 | 71.4 | 72.3 | 72.4 | 73.3 |
| $TiO_2$ | 0.28 | 0.27 | 0.34 | 0.42 | 0.38 | 0.59 | 0.54 | 0.39 | 0.62 | 0.43 | 0.44 | 0.39 | 0.36 |
| $Al_2O_3$ | 11.6 | 12.3 | 9.4 | 11.6 | 10.8 | 11.5 | 10.4 | 11.3 | 14.4 | 12 | 11.3 | 11.7 | 11.8 |
| $Fe_2O_3$ | 1 | 0.6 | 3 | 1.3 | 3.8 | 4 | 4.2 | 2.7 | 2.9 | 3.7 | 3 | 4.2 | 3.2 |
| FeO | 2.1 | 2.5 | 2.2 | 2.5 | 1.8 | 3.6 | 1.4 | 1.4 | 2.5 | 1.8 | 1.9 | 1.8 | 1.1 |
| MgO | 0.1 | 0.1 | 0.16 | 0.23 | 0.2 | 0.22 | 0.1 | 0.1 | 0.12 | 0.1 | 0.1 | 0.2 | 0.1 |
| CaO | 0.89 | 0.7 | 0.46 | 0.89 | 0.38 | 1.2 | 0.34 | 0.4 | 0.23 | 0.64 | 0.58 | 0.36 | 0.31 |
| $Na_2O$ | 3.7 | 4 | 3.1 | 3.5 | 2.6 | 5.2 | 4.6 | 4.3 | 5.8 | 4.8 | 4.6 | 5.3 | 4.1 |
| $K_2O$ | 4.1 | 4.2 | 4 | 4.6 | 4.9 | 4.3 | 4.3 | 4.5 | 5.7 | 4.3 | 4.8 | 2.7 | 5 |
| MnO | 0.13 | 0.1 | 0.17 | 0.11 | 0.05 | 0.3 | 0.18 | 0.21 | 0.13 | 0.18 | 0.22 | 0.15 | 0.13 |
| $P_2O_5$ | 0.05 | 0.05 | 0.05 | 0.05 | 0.05 | 0.05 | 0.05 | 0.05 | 0.05 | 0.05 | 0.05 | 0.05 | 0.05 |
| $H_2Op$ | 0.3 | 0.28 | 0.54 | 0.3 | 0.54 | 0.25 | 0.29 | 0.38 | 0.42 | 0.26 | 0.19 | 0.18 | 0.55 |
| $CO_2$ | 0.53 | 0.66 | 0.37 | 0.93 | 0.08 | 0.27 | 0.19 | 0.05 | 0.08 | 0.19 | 0.45 | 0.36 | 0.05 |
| Total | 99.88 | 99.76 | 99.49 | 99.73 | 99.68 | 99.78 | 99.89 | 99.98 | 99.85 | 99.85 | 99.93 | 99.79 | 100.05 |
| F | 1700 | 1300 | 1100 | 1200 | 2300 | 930 | 830 | 820 | 250 | 1300 | 810 | 540 | 250 |
| Cl | 20 | 20 | 20 | 20 | 20 | 20 | 20 | 20 | 20 | 20 | 20 | 20 | 20 |
| Agpaitic index | 0.91 | 0.9 | 1 | 0.93 | 0.89 | 1.15 | 1.17 | 1.06 | 1.09 | 1.05 | 1.13 | 0.99 | 1.03 |
| FeOt | 3 | 3.04 | 4.9 | 3.67 | 5.22 | 7.2 | 5.18 | 3.83 | 5.11 | 5.13 | 4.6 | 5.58 | 3.98 |
| Ba | 840 | 1080 | 200 | 390 | 300 | 740 | 600 | 440 | 670 | 510 | 340 | 690 | 300 |
| Nb | 81 | 95 | 350 | 130 | 170 | 50 | 52 | 53 | 88 | 77 | 50 | 110 | 56 |
| Cs | 6 | 5 | 5 | 5 | 5 | 5 | 7 | 6 | 18 | 5 | 5 | 5 | 5 |
| Rb | 110 | 110 | 160 | 82 | 160 | 75 | 75 | 68 | 77 | 88 | 72 | 64 | 84 |
| Hf | 15 | 21 | 68 | 27 | 22 | 10 | 8 | 9 | 13 | 12 | 8 | 17 | 8 |
| Sr | 68 | 87 | 29 | 73 | 25 | 55 | 18 | 33 | 14 | 40 | 19 | 59 | 13 |
| Y | 120 | 210 | 270 | 95 | 180 | 63 | 91 | 43 | 93 | 80 | 44 | 120 | 37 |
| Zr | 720 | 930 | 2690 | 1060 | 1050 | 390 | 370 | 360 | 590 | 600 | 340 | 830 | 400 |
| Ga | 32 | 34 | 29 | 35 | 36 | 41 | 37 | 42 | 52 | 37 | 40 | 43 | 41 |
| V | 8 | 8 | 8 | 8 | 8 | 8 | 8 | 8 | 8 | 8 | 8 | 8 | 8 |
| Th | 16 | 14 | 45 | 18 | 19 | 5 | 5 | 5 | 8 | 6 | 5 | 9 | 5 |
| U | 10 | 10 | 10 | 10 | 10 | 10 | 10 | 10 | 10 | 10 | 10 | 10 | 10 |
| Ta | 7 | 5 | 26 | 5 | 14 | 6 | 6 | 5 | 5 | 5 | 5 | 5 | 5 |
| Cu | 11 | 11 | 15 | 11 | 7 | 11 | 11 | 7 | 11 | 11 | 7 | 11 | 15 |
| Co | 28 | 28 | 28 | 28 | 28 | 23 | 34 | 23 | 34 | 28 | 28 | 39 | 28 |
| Ni | 29 | 18 | 18 | 41 | 24 | 24 | 18 | 129 | 41 | 47 | 18 | 18 | 24 |
| Cr | 52 | 26 | 77 | 103 | 52 | 52 | 39 | 258 | 90 | 65 | 52 | 39 | 39 |
| La | | 119.3 | | | 166.7 | | | | 79.88 | 76.29 | | 95.46 | |
| Ce | | 226.9 | | | 373.6 | | | | 182.9 | 170.9 | | 208.7 | |
| Nd | | 116 | | | 170.2 | | | | 87.14 | 70.1 | | 88.14 | |
| Sm | | 25.11 | | | 30.68 | | | | 15.58 | 14.54 | | 16.82 | |
| Eu | | 3.16 | | | 3.96 | | | | 2.43 | 2.25 | | 3.01 | |
| Gd | | 22.67 | | | 25.98 | | | | 10.86 | 10.81 | | 13.05 | |
| Dy | | 21.05 | | | 22.34 | | | | 7.4 | 9.16 | | 11.14 | |
| Ho | | 3.96 | | | 4.13 | | | | 1.33 | 1.72 | | 2.07 | |
| Er | | 9.41 | | | 9.45 | | | | 2.83 | 4.08 | | 4.77 | |
| Yb | | 7.02 | | | 6.42 | | | | 1.85 | 3.3 | | 3.09 | |
| Lu | | 0.89 | | | 0.82 | | | | 0.23 | 0.44 | | 0.39 | |
| ΣRare earth elements | | 555.47 | | | 814.28 | | | | 392.43 | 363.59 | | 446.64 | |

Table 4
Whole-rock analyses of the Couro de Onça intrusive suite

| Sample facies | 01C dyke | 01B isotropic | 01C1 dyke | 01D oriented | 01F dioritic dyke | 04A isotropic | 04B dyke | 12 isotropic | 7 isotropic | 13 isotropic | 56 isotropic | 57 isotropic | 02/II oriented | 04/II isotropic | 04A/II isotropic | 05/II oriented |
|---|---|---|---|---|---|---|---|---|---|---|---|---|---|---|---|---|
| $SiO_2$ | 79.63 | 77.04 | 73.56 | 70.84 | 72.47 | 76.4 | 71.89 | 70.43 | 74.77 | 74.55 | 77.83 | 74.22 | 71.84 | 76.25 | 76.73 | 67.8 |
| $Al_2O_3$ | 11.28 | 11.89 | 15.77 | 13 | 15.2 | 11.83 | 14.52 | 13.82 | 11.68 | 12.43 | 11.35 | 12.46 | 12.26 | 11.51 | 11.37 | 14.89 |
| $Fe_2O_3$ | 0.53 | 0.3 | 0.15 | 0.83 | 0.14 | 0.84 | 0.5 | 1.15 | 2 | 2.59 | 2.19 | 1.31 | 3.99 | 2.09 | 2.25 | 4.3 |
| FeO | 0.91 | 1.35 | 1.14 | 3.26 | 0.84 | 1.27 | 1.93 | 3.57 | 0 | 0 | 0 | 1.32 | 0 | 0 | 0 | 0 |
| CaO | 0.2 | 0.2 | 1.12 | 1.33 | 2.1 | 0.35 | 1.26 | 1.58 | 0.68 | 0.88 | 0.48 | 0.59 | 1.19 | 0.65 | 0.43 | 1.23 |
| MgO | 0.04 | 0.09 | 0.09 | 0.45 | 0.25 | 0.04 | 0.14 | 0.28 | 0.06 | 0.13 | 0.02 | 0.67 | 0.16 | 0.14 | 0.09 | 0.17 |
| MnO | 0.02 | 0.02 | 0.01 | 0.06 | 0.02 | 0.03 | 0.04 | 0.07 | 0.02 | 0.03 | 0.03 | 0.01 | 0.06 | 0 | 0 | 0.17 |
| $TiO_2$ | 0.18 | 0.18 | 0.13 | 0.46 | 0.07 | 0.23 | 0.18 | 0.59 | 0.21 | 0.29 | 0.21 | 0.38 | 0.39 | 0.21 | 0.20 | 0.46 |
| $Na_2O$ | 1.52 | 2.77 | 4.31 | 5.07 | 7.2 | 2.93 | 2.75 | 2.51 | 2.56 | 3.38 | 3.05 | 3.16 | 3.36 | 3.24 | 2.98 | 4.3 |
| $K_2O$ | 4.77 | 4.8 | 2.88 | 4.4 | 1.37 | 4.96 | 5.33 | 4.45 | 6.18 | 5.4 | 5.08 | 4.96 | 5.06 | 4.98 | 5.39 | 5.66 |
| $P_2O_5$ | 0.01 | 0.01 | 0.04 | 0.1 | 0.07 | 0.02 | 0.1 | 0.11 | 0.03 | 0.06 | 0.03 | 0.08 | 0.13 | 0.05 | 0.09 | 0.11 |
| $H_2Om$ | 0 | 0.02 | 0.2 | 0.04 | 0 | 0 | 0.15 | 0.13 | 0 | 0 | 0 | 0.15 | 0 | 0 | 0 | 0 |
| LOI | 0.09 | 0.48 | 0.43 | 0.37 | 0.48 | 0.15 | 0.47 | 0.41 | 0.45 | 0.46 | 0.44 | 0.7 | 0.42 | 0.56 | 0.3 | 0.5 |
| Total | 99.18 | 99.15 | 99.83 | 100.21 | 100.21 | 99.05 | 99.26 | 99.1 | 98.64 | 100.2 | 100.71 | 100.01 | 98.86 | 99.68 | 99.83 | 99.47 |
| FeOT | 1.39 | 1.62 | 1.27 | 4.01 | 0.97 | 2.03 | 2.38 | 4.6 | 1.8 | 2.33 | 1.97 | 2.5 | 3.59 | 1.88 | 2.02 | 3.87 |
| Agpaitic index | 0.68 | 0.82 | 0.65 | 1.01 | 0.88 | 0.86 | 0.71 | 0.65 | 0.93 | 0.92 | 0.93 | 0.85 | 0.9 | 0.93 | 0.94 | 0.89 |
| Cr | 89 | * | * | * | * | 87 | * | * | 13 | 15 | 14 | * | 3.94 | 3.86 | 2.88 | 2.63 |
| Ni | 17 | 17 | 19 | 16 | 19 | 20 | 17 | 18 | 16 | 0 | 0 | 18 | 1.39 | 2.09 | 2.72 | 1.84 |
| V | * | * | * | * | * | * | * | * | * | * | * | * | 3.59 | 0.96 | 0.57 | 4.85 |
| Zr | 299 | 286 | 53 | 365 | 78 | 363 | 162 | 497 | 343 | 364 | 433 | 390 | 442 | 467 | 466 | 564 |
| Co | 93 | 84 | 182 | 56 | 94 | 95 | 113 | 84 | 127 | 136 | 138 | 74 | 79.7 | 154 | 136 | 80.9 |
| Cu | * | 57 | 56 | 44 | 90 | * | 57 | 50 | 0 | 48 | 0 | 40 | 6.7 | 7 | 3.3 | 8.3 |
| Ga | 19 | 26 | 26 | 25 | 20 | 24 | 23 | 24 | 20 | 24 | 25 | 22 | 26.2 | 26.2 | 25.8 | 32.7 |
| Nb | 13 | 38 | 12 | 40 | 6 | 45 | 25 | 33 | 8.5 | 19 | 19 | 16 | 35.35 | 30.83 | 24.77 | 30.31 |
| Pb | 20 | 18 | 19 | 28 | 17 | 17 | 19 | 22 | 21 | 44 | 33 | 18 | 25.9 | 27 | 20.1 | 24.8 |
| Zn | 45 | 95 | 54 | 112 | 33 | 87 | 78 | 107 | 49 | 83 | 117 | 23 | 109 | 102 | 103 | 110 |
| Rb | 150 | 185 | 73 | 142 | 26 | 121 | 119 | 130 | 129 | 176 | 133 | 128 | 137.9 | 151.3 | 152.9 | 157.6 |
| Sr | 56 | 12 | 89 | 89 | 170 | 21 | 67 | 115 | 52.4 | 48.8 | 14.7 | 89 | 76.9 | 29.4 | 15.9 | 85.7 |
| Ba | 415 | 155 | 269 | 721 | 267 | 248 | 486 | 760 | 442 | 537 | 214 | 651 | 624 | 277 | 150 | 685 |
| F | 430 | 1600 | 640 | 1000 | * | 190 | * | * | | | | | | | | |
| Th | 22.69 | 17.39 | 7.77 | 13.52 | * | 16.77 | * | * | 20.4 | 18.7 | 20.4 | | 25.32 | 21.39 | 17.79 | 15.04 |
| U | 1.13 | 1.77 | 0.36 | 1.71 | * | 0.92 | * | * | 1.57 | 2.22 | 1.05 | | 1.65 | 1.82 | 0.97 | 1.24 |
| Y | 35 | 62 | 24 | 74 | * | 56 | * | * | 27 | 53 | 41 | | 71.3 | 53 | 51 | 55 |
| Hf | * | * | * | * | * | * | * | * | 9.9 | 11 | 12 | | 12.1 | 13.8 | 13 | 14.7 |
| Ta | * | * | * | * | * | * | * | * | 1.05 | 2.57 | 1.76 | | 2.67 | 2.44 | 1.87 | 1.99 |
| La | 116.1 | 72.8 | 35.4 | 56.7 | * | 115.9 | * | * | 95.9 | 73.7 | 60.2 | | 90.5 | 124.8 | 117.5 | 93.14 |
| Ce | 266.3 | 172.6 | 81.1 | 137.6 | * | 266.3 | * | * | 186 | 138 | 239 | | 180.8 | 242.3 | 230.3 | 187.1 |
| Pr | 24.77 | 16.75 | 7.62 | 13.65 | * | 25.4 | * | * | 19.89 | 15.83 | 13.7 | | 20.92 | 27.49 | 26.34 | 21.2 |
| Nd | 105.1 | 76 | 33.8 | 63.9 | * | 111.7 | * | * | 75 | 62 | 52.7 | | 76.84 | 98.56 | 95.95 | 75.73 |
| Sm | 17.5 | 14.8 | 6.4 | 12.6 | * | 18.6 | * | * | 12.6 | 12.1 | 11.2 | | 14.49 | 17.03 | 17.75 | 13.76 |
| Eu | 1 | 0.67 | 1.07 | 2 | * | 1.02 | * | * | 1.391 | 1.397 | 0.873 | | 1.9 | 1.17 | 0.89 | 2.25 |
| Gd | 15.3 | 13.7 | 5.8 | 12.8 | * | 16.7 | * | * | 8.98 | 10.4 | 9.41 | | 12.74 | 13.25 | 14.3 | 11.72 |
| Tb | 1.9 | 2.1 | 0.9 | 2 | * | 2.2 | * | * | 1.27 | 1.75 | 1.65 | | 2.06 | 2 | 2.06 | 1.89 |
| Dy | 7.8 | 11 | 4.5 | 11.8 | * | 11.2 | * | * | 6.31 | 9.95 | 8.81 | | 11.69 | 10.6 | 10.88 | 10.05 |
| Ho | 1.3 | 2.1 | 0.8 | 2.4 | * | 2 | * | * | 1.04 | 1.89 | 1.62 | | 2.6 | 2.22 | 2.08 | 2.11 |
| Er | 3.2 | 6 | 2.3 | 7.5 | * | 5.7 | * | * | 2.83 | 5.56 | 4.61 | | 6.62 | 5.08 | 4.82 | 5.52 |
| Tm | 0.35 | 0.73 | 0.29 | 0.97 | * | 0.69 | * | * | 0.359 | 0.808 | 0.613 | | 1 | 0.73 | 0.62 | 0.84 |
| Yb | 1.9 | 4.2 | 1.7 | 7 | * | 4.2 | * | * | 1.69 | 4.8 | 3.66 | | 5.89 | 4.67 | 3.77 | 4.64 |
| Lu | 0.31 | 0.63 | 0.26 | 1.17 | * | 0.64 | * | * | 0.243 | 0.661 | 0.509 | | 0.92 | 0.68 | 0.62 | 0.69 |
| ΣRare earth elements | 562.83 | 394.08 | 181.94 | 332.09 | * | 582.25 | * | * | 390.94 | 318.57 | 390.97 | | 402.39 | 518.14 | 496.78 | 404.6 |

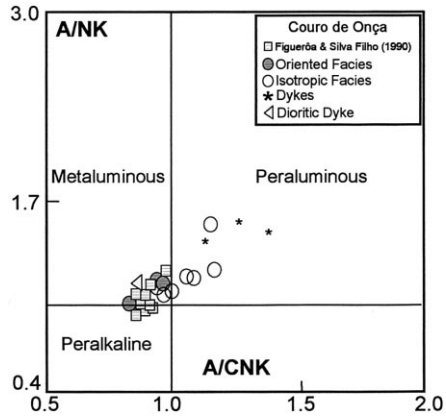


Fig. 5. Al(Na + K) vs. Al/(Ca + Na + K) diagram (Maniar and Piccoli, 1989) to discriminate peralkaline, metaluminous, and peraluminous rocks.

rocks belonging to the strongly peralkaline group, as shown by agpaitic index values in Table 3. Alkaline saturated to oversaturated complexes display associated metaluminous and peralkaline types (Bonin, 1988). In this context, the SMS represents a typical example of this association.

The agpaitic index and FeO/(FeO + MgO) ratio are very useful indicators of alkaline signature in silica-oversaturated rocks (Fig. 6). In this context, both suites plot in the field of alkaline granites. Two samples from the COIS show subalkaline character, 01F (quartz monzodioritic dyke) and 57 (biotite syenogranite; Fig. 6). Macroscopic and petrographic observations indicate that sample 01F represents contaminated liquid, whilst the biotite syenogranitic sample is strongly transformed by hydrothermal processes, evident as plagioclase and biotite transformation to epidote, and occasionally into white mica. Then, the chemical composition of these samples probably does not represent the liquid composition during crystallization. Other six samples plot below the field of alkaline granites, although they were considered to have alkaline affinity. As evidenced by Nardi (1991), this field includes more than 80% of the alkaline granites, although it is usual to find some granites which plot below. The high FeO/(FeO + MgO) ratio in alkaline suites is due to their high FeOt contents, associated with extremely low MgO concentrations in these magmas (Sorensen, 1974; Whalen et al., 1987), as evidenced by the absence of Mg-rich minerals, since biotites are normally Fe-rich.

### 5.1. Major elements

The extremely high $SiO_2$ contents represent an obstacle to determinate the geochemical affinity of granitic rocks, as observed by Mahood and Hildreth (1983). On the other hand, major element contents are diagnostic for alkaline granites (Whalen et al., 1987; Nardi, 1991).

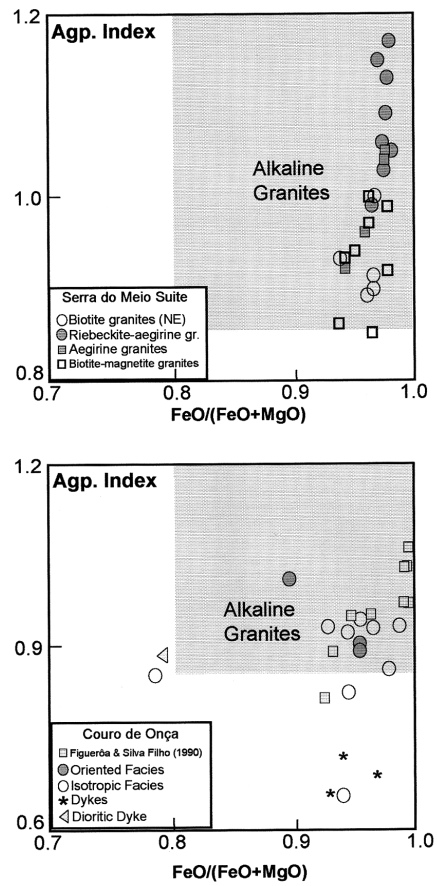


Fig. 6. Agpaitic index vs. FeOt/(FeOt + MgO) ratio diagram, according to Nardi (1991), showing the usual field for alkaline granites.

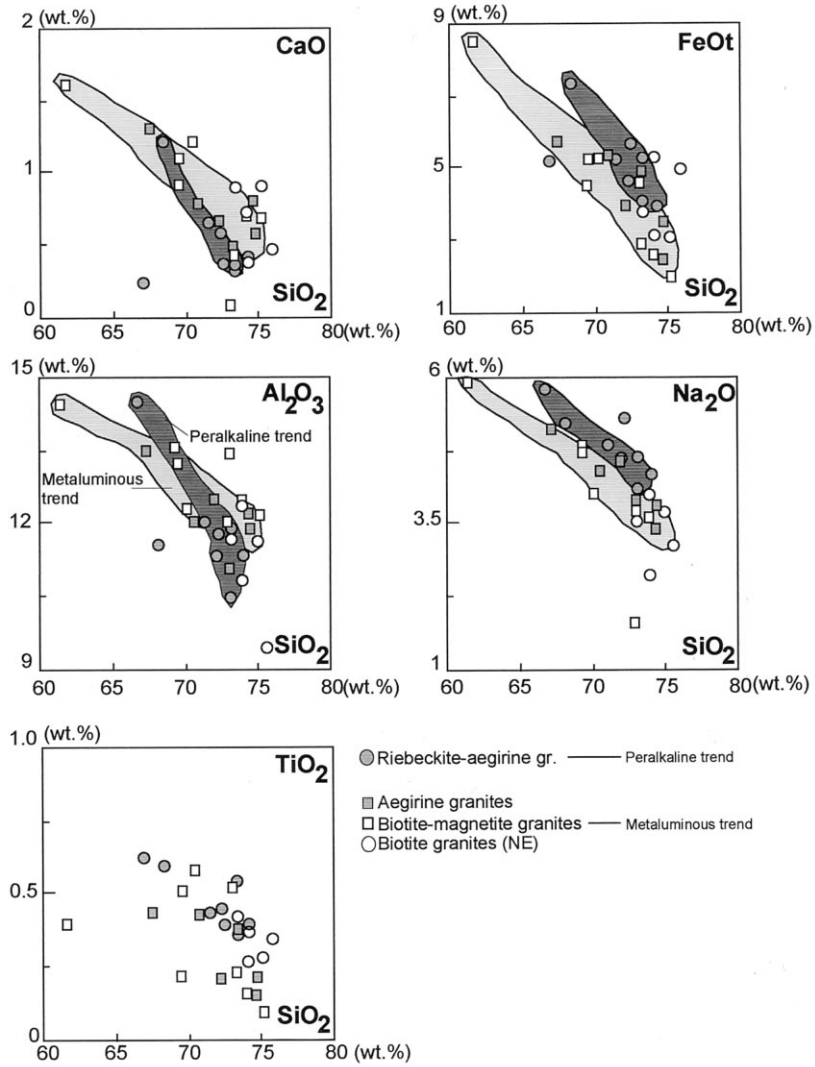


Fig. 7. Harker type diagrams (in wt.%) for SMS, showing in some cases the parallel evolutionary lines between peralkaline and metaluminous trends.

Saturated to oversaturated rocks of this magmatic series have very low contents of MgO and CaO, medium concentrations of $Al_2O_3$, and high contents of $Na_2O$, $K_2O$, FeOt, and FeOt/(FeOt + MgO). The COIS present generally higher $Al_2O_3$ (11.28–15.77 wt.%) and CaO (0.20–1.58 wt.%) contents than the SMS (9.4–13.5 and 0.3–1.2 wt.%, respectively), for samples with similar $SiO_2$ contents. Bonin (1987) showed that calcium, in granites, progressively decreases from late to anorogenic phases of a tectonic event. In fact, as previously discussed, COIS granites have a late-Transamazonian age, while the SMS, is probably a typical alkaline anorogenic suite.

Major elements show similar behaviour to that described by Mahood and Hildreth (1983), Miller and Mittlefehldt (1984) for high-$SiO_2$ granitic liquids, with most decreasing during magmatic evolution (Figs. 7 and 8). In Harker-type diagrams (Fig. 7), the SMS evolves according to two parallel

paths in terms of $Al_2O_3$, FeOt, CaO, and $Na_2O$, for similar $SiO_2$ contents, (i) metaluminous and slightly peralkaline granites, forming the metaluminous trend, and (ii) strongly peralkaline granites, forming the peralkaline trend. Their evolution, considering similar range of $SiO_2$ contents, is indicative of the presence of two different alkaline parental liquids, and/or probably reflecting differences in source composition. The peralkaline trend has higher contents of FeOt, $Na_2O$, and $TiO_2$, with lower CaO and $Al_2O_3$, for similar $SiO_2$ values, relative to the metaluminous trend (Fig. 8). The parallelism between the two trends is indicative of similar magmatic evolution during crystallization of metaluminous and peralkaline rocks, although the $Al_2O_3$ versus $SiO_2$ plot suggests more intense feldspar fractionation in the metaluminous liquids to produce the more differentiated granites.

In the COIS, $Al_2O_3$ behaviour reflects a constant decrease of plagioclase modal proportions with increasing differentiation (Fig. 8). The dykes have higher $Al_2O_3$ contents and lower concentrations of FeOt, MgO and $TiO_2$ than the granites for similar $SiO_2$ values, which is in agreement with their more leucocratic character. Most elements show linear or exponential decrease during evolution from foliated to isotropic granites (Fig. 8), which indicates fractionation of plagioclase (Ca, Na, and Al decrease) and amphibole (Ca, Fe, and Mg).

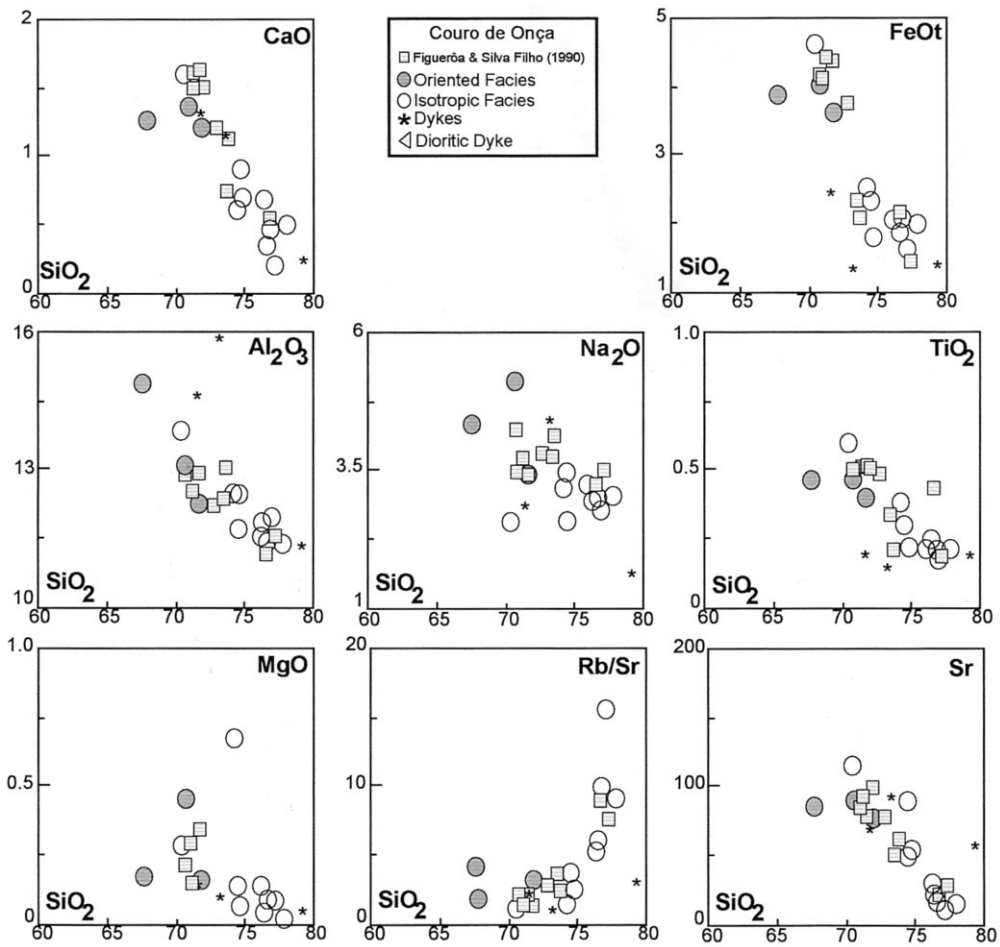


Fig. 8. Harker type diagrams of the COIS.

### 5.2. Trace elements

Alkaline granites present high HFSE concentrations, such as Zr, Nb, Y, Ga, and REE (Collins et al., 1982; Whalen et al., 1987; Bonin, 1988), associated with depletion of Sr, Ba, Cu, V, Cr and Ni, due to their strongly evolved character. As studied by Watson (1979), in metaluminous liquids, zircon saturation is attained at less than 100 ppm of Zr, whereas Zr solubility increases in peralkaline liquids (Watson, 1979; Watson and Harrison, 1983). These results have pointed out that Zr solubility is a function of agpaitic index. According to the same authors, high temperature of the melt can increase Zr solubility.

#### 5.2.1. Serra do Meio suite

Trace elements at these granites were previously studied by Leite (1993), Plá Cid (1994), Plá Cid et al. (1997a). These rocks are characterized by high contents of Zr (340–2690 ppm), Ga (29–53 ppm), Y (37–270 ppm), Nb (50–350 ppm), Hf (8–68 ppm), F (250–4100 ppm), and Ce (114–474 ppm); medium concentrations of Ba (77–1310 ppm) and Rb (64–280 ppm), and depletion of Cr (26–258 ppm), Ni (12–129 ppm), and Sr (13–140 ppm). Incompatible elements display contents generally above the average concentrations of alkaline granites, when compared with typical suites studied by Bonin (1980), Bowden and Kinnaird (1984), Whalen et al. (1987).

Zirconium exhibits unusual behaviour, with higher contents in the metaluminous trend granites (260–2690 ppm) than in the peralkaline one (340–830 ppm; Plá Cid et al., 1997a,b). Zr has been used by Bowden and Turner (1974), Bonin (1988) as a peralkalinity index indicator, a procedure also followed in this paper (Fig. 9). This unusual behaviour is followed by strong enrichment in HFSE and rare earth elements (REE) in the metaluminous trend relative to the peralkaline one (Fig. 9). This behaviour is completely opposite to that expected for typical alkaline granitic suites, where incompatible elements are enriched in the peralkaline terms. This unusual behaviour may be explained by two different possibilities, (i) metaluminous and peralkaline granites are produced from different sources, or (ii) both granite types were produced from liquids generated by successive extraction from the same source.

The behaviour of Ga is related, according to Whalen et al. (1987), to the agpaitic index of granites, with higher contents present in peralkaline types. In the Serra do Meio granites, Ga is above the average values for peralkaline granites, such as the peralkaline granites from Corsica (Bonin, 1980, 1982, 1988), alkaline granites from Nigeria (Bowden and Kinnaird, 1984), and from a $SiO_2$-saturated peralkaline volcanic–plutonic association from New Mexico (Czamanske and Dillet, 1988; Fig. 9). In Fig. 9, the SMS has comparable composition to these typical alkaline suites, although it presents higher amounts of incompatible elements. This confirms that the SMS granites have a chemical composition typical of alkaline magmatic suites, in spite of deformation/recrystallization processes to which they have been submitted during the Brasiliano cycle.

Rb/Sr versus Sr, Rb and Ba plots (Fig. 10) permit separation of the metaluminous and peralkaline trends. The parallelism between these trends suggests that the magmatic evolution is very similar. Since these granites do not contain plagioclase crystals, it is probable that Sr decrease reflect alkali-feldspar fractionation. These plots may be interpreted as suggestive of a metaluminous trend generated from a parental liquid rich in Rb and Sr. The strong Ba decrease in the metaluminous trend, less intense than in the peralkaline one, indicates a stronger alkali-feldspar fractionation in this evolutionary line.

#### 5.2.2. Couro-de-Onça intrusive suite

These granites, excluding samples 01F and 57, show trace-element concentrations which are consistent with the alkaline series. They are characterized by medium to high values of Rb/Sr (1–15), Rb (73–218 ppm), Ga (19–32 ppm), Nb (12–45 ppm), Zr (53–688 ppm), Y (24–84 ppm), F (190–1600 ppm), and Ce (81–266 ppm), and low contents of Sr (12–89 ppm), Ba (155–760 ppm), Cr ($< 89$ ppm), and Ni ($< 20$ ppm).

LIL-element variation confirms the alkali-feldspar and plagioclase importance during the COIS magmatic evolution (Fig. 8). This evolution is controlled by plagioclase fractionation, princi-

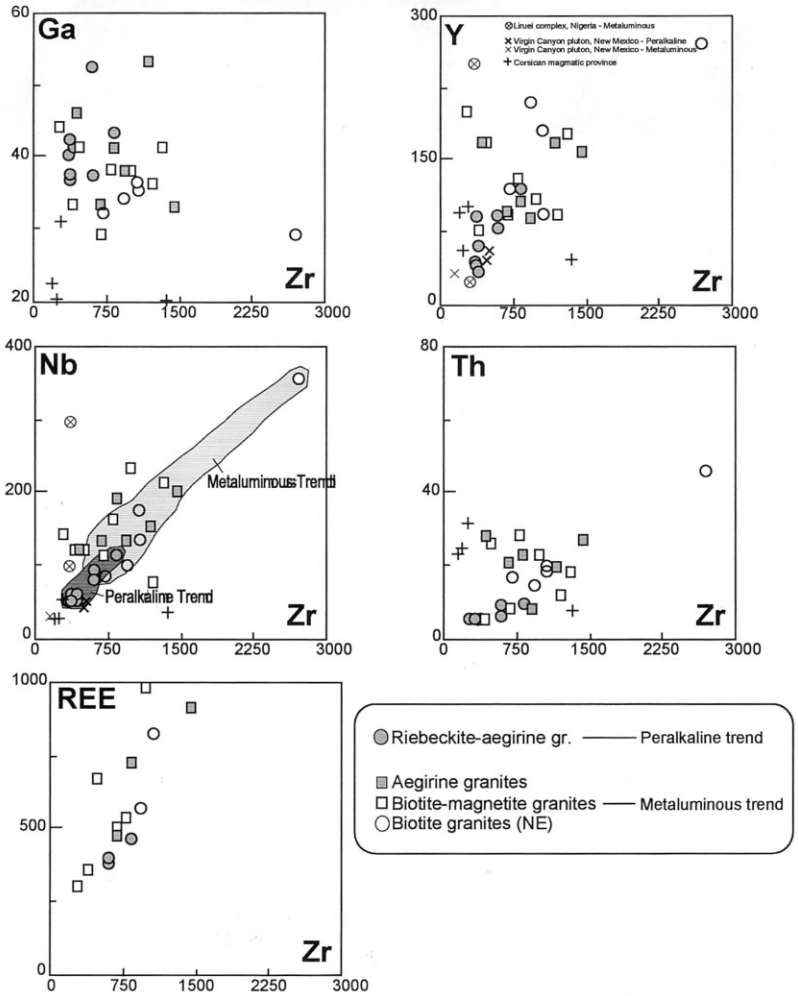


Fig. 9. Zr (in ppm) vs. Ga, Y, Nb, Th, and REE (in ppm) plots showing the different contents between peralkaline and metaluminous trends in the SMS. Corsican magmatic province analysis are from Bonin (1980), in the Liruei complex from Bowden and Kinnaird (1984) and to the New Mexico volcanic–plutonic association from Czamanske and Dillet (1988).

pally around 73 wt.% of $SiO_2$, as demonstrated by Rb/Sr and Sr evolution with differentiation (Figs. 8 and 11). Sr shows strong compatible behaviour, which is in agreement with plagioclase fractionation during the magmatic evolution of this suite. Rb/Sr versus MgO, FeOt, and $TiO_2$ diagrams (Fig. 11) suggest amphibole fractionation, as well as Fe–Ti oxide, during magmatic evolution.

### 5.3. Rare earth elements

Rare earth elements (REE) were normalised to the chondritic values of Evensen et al. (1978), and patterns displayed in Fig. 12. Serra do Meio and Couro-de-Onça intrusive suites have very similar patterns, with heavy REE fractionation relative to the light ones, and pronounced, negative Eu anomalies.

*5.3.1. Serra do Meio suite*

The REE patterns are parallel or roughly parallel, with pronounced, negative Eu anomaly (Fig. 12). $Ce_N/Yb_N$ fractionation ratios are lower in the NS-oriented metaluminous plutons ($Ce_N/Yb_N$, 8.97–16.16) than in the strongly peralkaline granites (14.38–27.46). The slightly peralkaline and metaluminous, magnetite-bearing facies have fractionation ratios similar to those of riebeckite-bearing facies (Plá Cid, 1994). Nevertheless, the metaluminous rocks have higher total REE concentrations than the strongly peralkaline granites (Fig. 12). The negative Eu anomalies increase from the strongly peralkaline granites ($Eu/Eu^* = 0.52–0.60$) to the NS-oriented metaluminous plutons ($Eu/Eu^* = 0.40–0.42$). These anomalies are more pronounced in the slightly peralkaline facies (0.25–0.38), the metaluminous, magnetite-bearing plutons presenting larger variation, from 0.13 to 0.57. The metasomatically altered granites show light REE-enrichment and high ($Ce_N/Yb_N$) ratios, which according to Plá Cid (1994), is due to REE transport by fluids associated with the tectonic events related to the Brasiliano cycle.

The Serra do Meio granites are REE enriched when compared with the average contents presented by Bowden and Whitley (1974) for alkaline metaluminous and peralkaline granites. The negative Eu anomalies increasing from peralkaline to metaluminous trend, associated with trace elements evolution (Fig. 9), suggest differences either in the magmatic evolution, or in the sources, of peralkaline and metaluminous magmas of this suite.

*5.3.2. Couro-de-Onça intrusive suite*

Rare earth element patterns in the COIS (Fig. 12) show an evolution from the foliated to the isotropic types, characterized by higher ($Ce_N/Yb_N$) ratio in the more evolved rocks (11.41–18.13), whereas in the granites with $SiO_2$ around 70 wt.%, it ranges from 5.46 to 11.20. This variation is due to heavy REE-enrichment, possibly attributed to higher modal concentrations of apatite, that may readily accommodate these elements (Wilson, 1989), and as suggested by positive correlation between $P_2O_5$ and Yb (Fig. 13). The total REE-contents are extremely vari-

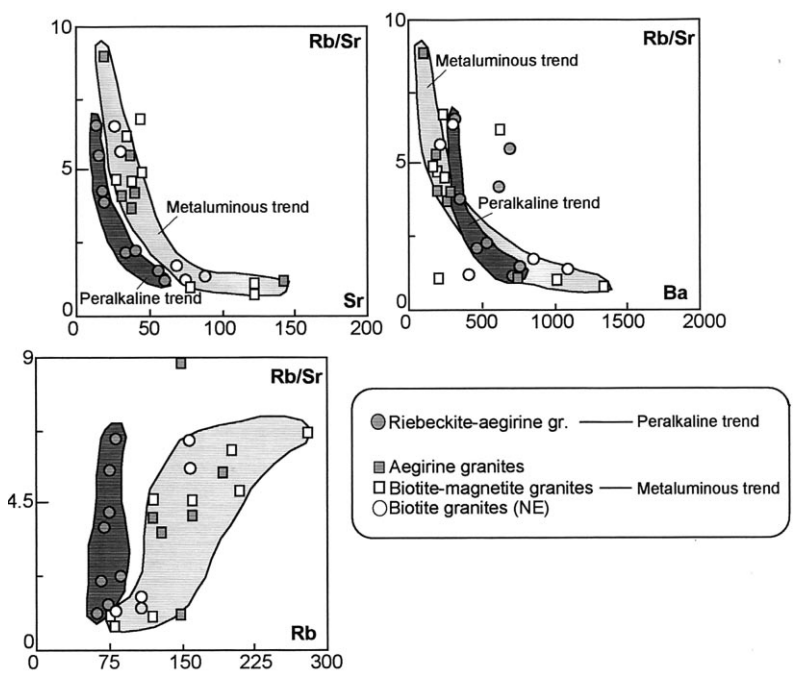


Fig. 10. Rb/Sr vs. Sr, Ba, and Rb (in ppm) plots for the SMS.

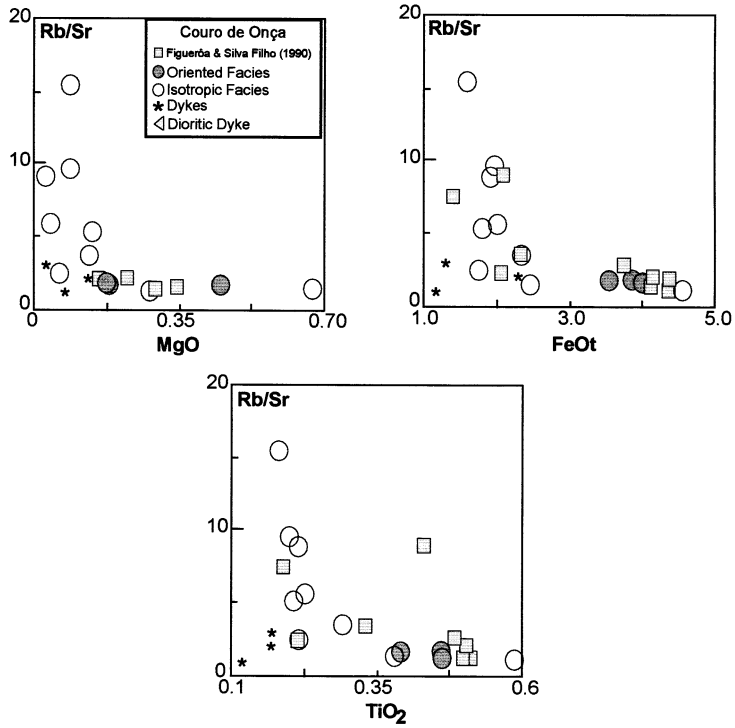


Fig. 11. Rb/Sr vs. FeOt, MgO, and $TiO_2$ plots of the COIS, suggesting fractionation of amphibole, Fe–Ti oxide, and plagioclase during the magmatic evolution.

able, and are not related to $SiO_2$ increase. Both foliated and isotropic facies have negative Eu anomalies, which are lower in the foliated rocks, and increase with differentiation (Fig. 12). This is probably related to plagioclase modal decrease from foliated types to less or non-foliated ones, suggesting plagioclase fractionation. These REE patterns are similar to those found in the alkaline and Rapakivi granites from the Amazonian province (Fig. 12; Dall'Agnol et al., 1994).

## 6. Discussion

### 6.1. Emplacement and tectonic setting

Alkaline granites are commonly emplaced during the late stages of an orogenic event, or immediately after it, and in anorogenic settings, as described by Bonin (1987), Nardi and Bonin (1991), Don Hermes and Zartman (1992). In the COIS, the foliation of the granites parallel to the regional deformation structures is suggestive of their late-tectonic emplacement. According to Figuerôa and Silva Filho (1990), these granites are emplaced during the late stages of a transcurrent event attributed to the Transamazonian cycle. On the other hand, the Rb–Sr isochron for the SMS (850–500 Ma), associated with field data, is compatible with a pre-Brasiliano emplacement of this suite (Plá Cid, 1994). Its association with Transamazonian carbonatitic rocks and tholeiitic to transitional basalts with preserved cumulate textures (Couto, 1989) points to an extensional, intracontinental tectonic setting during emplacement of this magmatic province. The enrichment of incompatible elements, such as Zr, Nb, Y, Ga, and light REE, relative to the average of anorogenic granites (Whalen et al., 1987), and to anorogenic suites, such as the Corsican (Bonin, 1980, 1988) and the Amazonian provinces (Dall'Agnol et al., 1994) put in evidence the anoro-

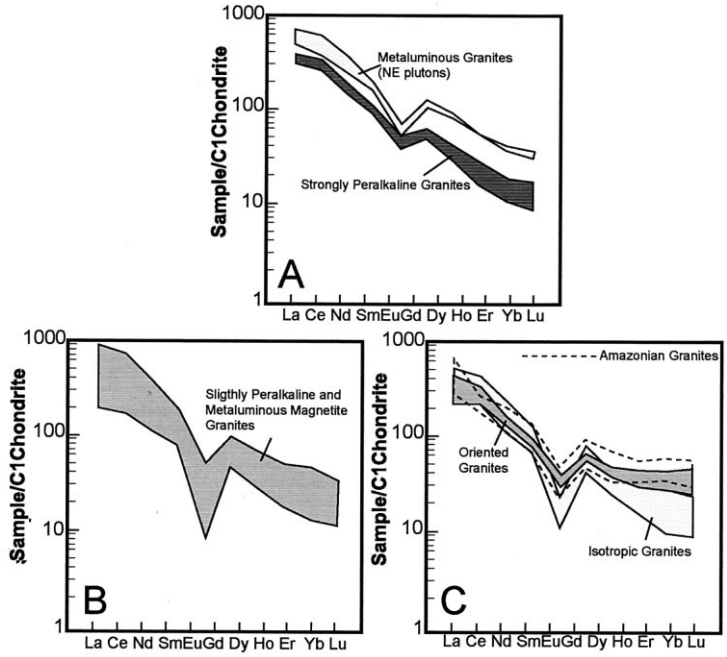


Fig. 12. REE patterns of the SMS (A, B) and COIS (C), normalised to chondritic values (Evensen et al., 1978). Amazonian granites patterns are from Dall'Agnol et al. (1994).

genic character of these alkaline granites and their anomalous enriched source. Pearce et al. (1984) used trace-element diagrams to discriminate different tectonic settings. For both suites, the trace-element contents plot in the field of within-plate granites (Fig. 14). In the COIS, the dykes have very low trace-element concentrations, due to intense fractionation of accessory phases.

### 6.2. Crystallization and recrystallization

The SMS rocks are affected strongly by solid-state deformation, with intense recrystallization. However, some magmatic textures are preserved, such as alkali-feldspar phenocrysts and some mafic minerals, such as arfvedsonitic amphiboles, aegirine–augite, and Ti-aegirine, which have subhedral igneous forms and primary mineral compositions. According to Silva (1987), Jardim de Sá (1994), the metamorphic temperatures estimated for the Riacho do Pontal fold belt, and particularly in the Campo Alegre de Lourdes region, range from greenschist to low amphibolite facies. This is confirmed by the textural relations observed in these granitic rocks. The annealing of quartz, observed in all facies, reflects static, post-deformational, thermal effects (Hibbard, 1995), and represents the lower limit of recrystallization temperatures. On the other hand, the newly-formed feldspars, and recrystallization of sodic

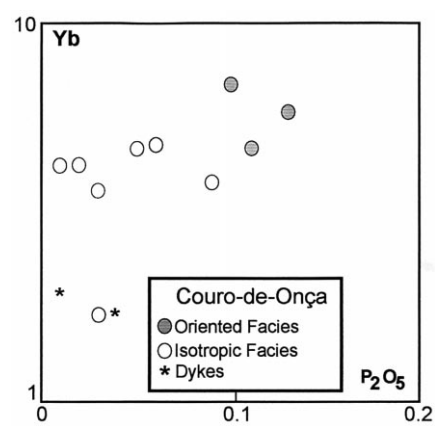


Fig. 13. $P_2O_5$ (in wt.%) vs. Yb (in ppm) plot of the COIS.

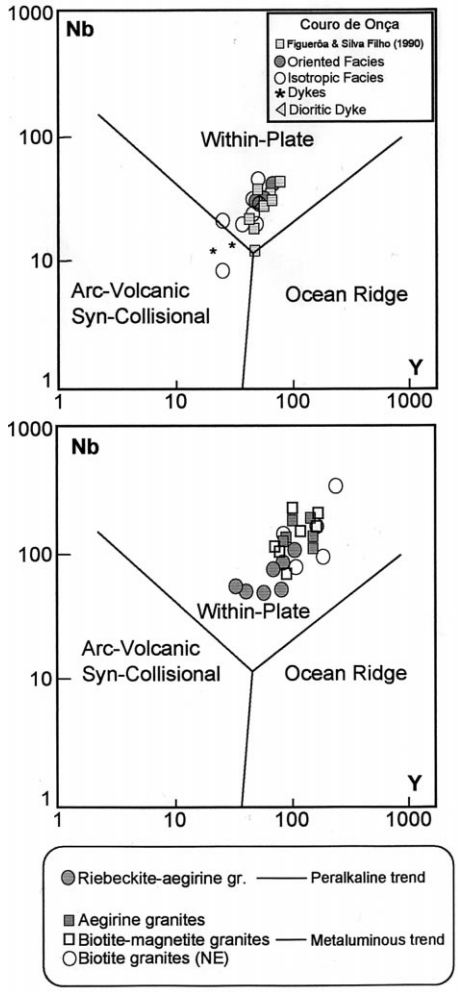


Fig. 14. Nb (in ppm) vs. Y (in ppm) plot, with tectonic setting fields for granitic rocks based on Pearce et al. (1984).

mafic minerals represent the highest temperatures attained during the Brasiliano cycle. This limit can be estimated from the stability conditions of alkali amphiboles (Ernst, 1962). This author shows that, for high $fO_2$ conditions, riebeckite is the only sodic amphibole stable around 520°C, as also observed by Bonin (1982), which provides evidence that riebeckite is a typical alkali-amphibole formed at subsolidus temperatures. Thus, the upper metamorphic temperature limit is probably below 550°C. The occurrence of calcite crystals suggests that recrystallization condition was in presence of $CO_2$-rich fluids, which might have enhanced ductility during deformation.

Irregular-shaped remnants of plagioclase in alkali-feldspar grains are taken as evidence of partial resorption texture in the COIS. Furthermore, the subhedral character of alkali-feldspar and plagioclase grains, and the relative absence of inclusions, suggest they have crystallized at the same time in the less differentiated rocks. Based on experimental studies by Luth and Tuttle (1966), the occurrence of perthitic feldspar with microcline borders is compatible with a minimum solidus temperature of 650°C. According to Neksvasil (1992), the simultaneous crystallization of alkali-feldspar and plagioclase, with intensive plagioclase partial resorption, in $SiO_2$-saturated liquids, occurs at about 950°C, whereas for plagioclase initial crystallization the inferred temperatures may reach up to 1100°C. These experiments have been conducted at 5 kb, and at lower pressures would result in less than 10% variation. The mineral orientation, with irregular, curved and interpenetrating contacts, point to crystallization controlled by a regional stress field, which is corroborated by Pb–Pb in zircon isotopic data of $2157 \pm 5$ Ma, confirming the late-orogenic character of this suite.

In the COIS, disequilibrium textures might result from changes in conditions of $P_{fluids}$ and total pressure, caused by intrusion of the dyke swarm, with intense fluid percolation in the host granites. Since reversal zoning in amphibole, as well as microgranular concentrations are more commonly observed in more differentiated granites, it is evident that the granitic liquid was partially crystallized. Then, during differentiation of this granitic magma, fracturing was probably controlled by regional deformation. This supposition is supported by parallelism between coarse grain dykes and banding in granites, as well as by a similar orientation of amphiboles in dykes and granites.

### 6.3. Possible nature of the source

Trace elements have been employed by Pearce and Norry (1979), Pearce et al. (1984), Wilson (1989), among others, to establish constraints on the possible mantle or crustal derivation of granitic magmatism, as well as on its tectonic

setting. Spiderdiagrams normalised to the ocean ridge granite (ORG) values (Pearce et al., 1984) for the SMS granites are shown in Fig. 15. Their high Nb and Ta contents, and the similar concentrations of Rb and Th with respect to the ORG values, are typical OIB-type mantle features (Pearce et al., 1984; Wilson, 1989). Plá Cid et al. (1997a,b) concluded that they derived from an incompatible-element enriched mantle source. The peralkaline trend of the SMS is less enriched in HFSE, whereas the metaluminous one is strongly enriched in Rb, Th, Nb, and Ta, with large, negative Ba anomaly (Fig. 15). The negative Ba anomaly explains the more pronounced Eu negative anomaly in the metaluminous trend granites, which is probably due to intense feldspar fractionation during magmatic evolution, less evident in peralkaline ones. The high Rb and Th contents are suggestive of crustal contamination (Thirwall and Jones, 1983), although, as shown in tectonic settings diagrams of Pearce et al. (1984), within-plate granites exhibit enrichment in Rb with increasing Nb contents. Dooley and Patiño Douce (1996), Patiño Douce and Beard (1996) showed by experimental studies the improbability of crustal sources to generate peralkaline granitic compositions.

Trace element contents of COIS, normalized to the ORG (Pearce et al., 1984; Fig. 15), show a typical within-plate pattern. There are some examples of granites in Brazil with similar geochemical affinities, generally emplaced in extensional continental settings, such as the Proterozoic anorogenic granitoids from Central Amazonian province (Dall'Agnol et al., 1994), and the post-orogenic monzo-syenogranites of Jaguari pluton, from the Saibro Intrusive Suite, southern Brazil (Gastal and Nardi, 1992).

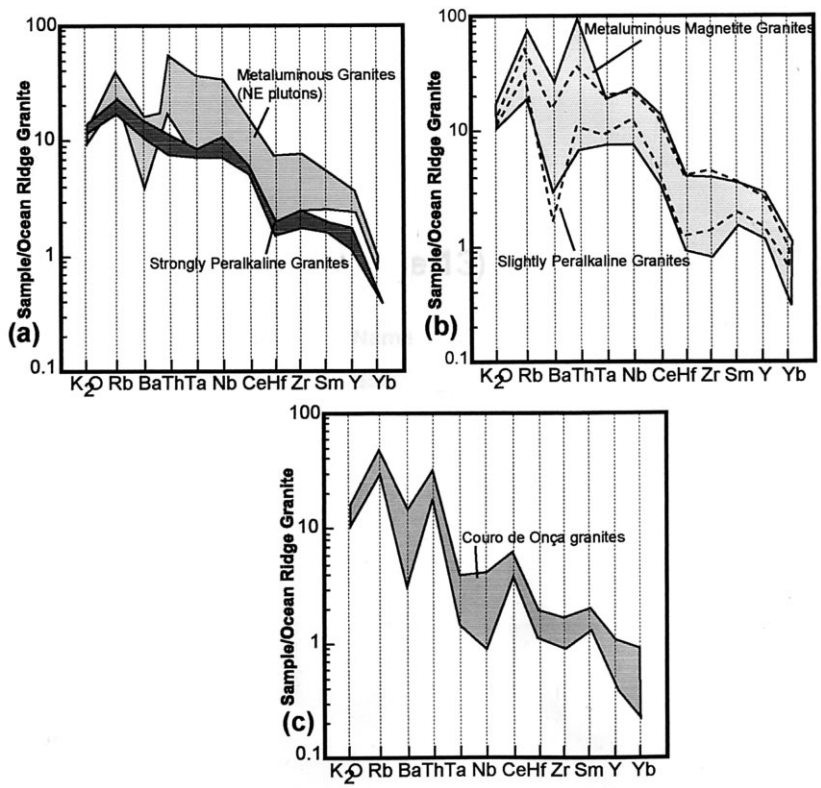


Fig. 15. Spidergrams of the Serra do Meio (a, b) and Couro de Onça (c) suites normalised to Ocean Ridge granites (Pearce et al., 1984).

Jacobson et al. (1958) proposed a genetic model, modified by Bowden and Kinnaird (1978), to explain the evolution of alkaline suites, mainly for their acid components. This model proposes an evolution from olivine-gabbro to syenite and fayalite-granite through plagioclase dominated fractionation, generating anorthosite cumulates. From fayalite-granite, two different paths begin due to fractional crystallization processes, a peralkaline trend, producing arfvedsonite and riebeckite granite, and an aluminous line, responsible for hastingsite and biotite granites. Bonin (1982) presents a similar scheme, where syenitic/monzonitic rocks evolve to peralkaline and peraluminous lines. In this scheme, hastingsite granites are the less evolved rocks in the peralkaline trend.

Two different hypotheses can explain the trace element concentrations of metaluminous and strongly peralkaline granites from the SMS. Firstly, both granitic types were produced by partial melting from different sources. This model would hardly explain the linear trend observed for some pairs of trace elements in Fig. 9. Furthermore, different sources neither explain the alkaline signature of both granite types, nor similar ratios of elements such as Zr/Nb, Y/Zr, La/Sm, and Dy/Yb. Secondly, two different parental basic melts were produced by extraction, through a small degree of partial melting, of the mantle at different stages. If this is accepted, an original melt responsible for the evolution towards metaluminous trend was the first magma type extracted, with the solubility of Zr enhanced by high temperature and F contents. This initial magma extraction could have caused a relative depletion in these elements at the source, directly affecting the composition of peralkaline liquids generated during a second partial-melting event.

In the specific case of granites from the SMS, the unusual concentrations of incompatible elements in the metaluminous trend can be explained in terms of F contents. In fact, the granites of metaluminous trend are strongly enriched in incompatible elements when compared with typical anorogenic metaluminous granites from Nigeria (Bowden and Kinnaird, 1984), but they are also enriched in F. According to Harris (1980), high alkali contents in magmas promotes F enrichment and, consequently, the presence of halogens is responsible for stabilization of Zr, Nb, Y, and Th complexes, which are the enriched elements in the studied metaluminous granites. According to Watson (1979), high alkali contents in liquids with low F promote the formation of alkali-zirconosilicate complexes ($Na_4Zr(SiO_4)_2$) and, as assumed by Bonin (1988), the presence of ns (Na-silicate) in the CIPW norm is a good indicator of alkali-zirconosilicate complexes. In the SMS, ns absence in the CIPW norm (Table 5) suggests the probable formation of F–Zr complexes. As can be seen in Table 3, the metaluminous trend is F-richer than the strongly peralkaline ones, where F content in the former ranges from 300–4100 ppm (values are usually $>1100$ ppm), and from 250 to 1300 ppm in the latter. This may be suggestive of metaluminous trend being related to the first partial melting stage, which promoted the stabilization of F-rich complexes due to high alkali contents of the original melt, consequently transporting elements such as REE, Nb, Zr, Y, and Th.

Similar control on HFSE and REE behaviour by F-rich complexes was demonstrated by Charoy and Raimbault (1994) in biotite granites of alkaline affinity from eastern China, extremely enriched in these elements. According to these authors, the magmatic evolution of these granites was controlled by F-rich, water-poor, high-temperature magmas, which become volatile-saturated late in the crystallization sequence. The positive correlation between HFSE and F indicates that these fluids have complexed and transported HFSE as soluble components.

It is concluded that SMS metaluminous and peralkaline trends reflect the evolution of two parental magmas, successively extracted from the same enriched mantle source. Both alkaline lines evolved from alkali-basalt liquids, mainly through crystal fractionation processes. Metaluminous-trend rocks evolved from a Ca-richer magma, whereas the strongly peralkaline granites were produced from a Na, Ti, and Fe enriched liquid.

Finally, it is concluded that the two different alkaline granites suites, which occur at the northern border of the São Francisco Craton, have been emplaced in a within-plate tectonic setting, during extensional tectonic regimes related to the

Table 5
CIPW norm of the Serra do Meio suite

| Sample | CL-05b | CL-105 | CL-54 | CL-55 | GA-13 | CL-16 | GA14c | GA-34 | GA-39 | GA-46 | GA-46a | TR-72 | PPB-78a | | | |
|---|---|---|---|---|---|---|---|---|---|---|---|---|---|---|---|---|
| Quartz | 35.28 | 31.78 | 41.71 | 32.72 | 39.62 | 19.89 | 31.57 | 31.95 | 11.2 | 26.8 | 27.21 | 31.11 | 30.76 | | | |
| Corundum | – | 0.02 | – | – | 0.65 | – | – | – | – | – | – | – | – | | | |
| Orthoclase | 24.46 | 25.11 | 23.98 | 27.6 | 29.23 | 25.6 | 25.56 | 26.71 | 33.9 | 25.56 | 28.57 | 16.08 | 29.71 | | | |
| Albite | 31.61 | 34.25 | 26.44 | 30.06 | 22.21 | 35.45 | 29.71 | 33.19 | 42.58 | 37.99 | 31.6 | 45.18 | 33.01 | | | |
| Anorthite | 2.95 | 3.18 | – | 2.38 | 1.57 | – | – | – | – | – | – | 0.15 | – | | | |
| Acmite | – | – | 0.15 | – | – | 7.82 | 8.32 | 2.95 | 6 | 2.53 | 6.69 | – | 1.65 | | | |
| ns | – | – | – | – | – | – | – | – | – | – | – | – | – | | | |
| Diopside | 1.04 | – | 1.7 | 1.54 | – | 4.97 | 1.18 | 1.43 | 0.72 | 2.44 | 2.26 | – | – | | | |
| Hypersthene | 2.54 | 4.13 | 0.9 | 2.85 | 0.5 | 3.08 | 0.55 | 0.44 | 3.06 | – | 1.67 | 0.5 | 0.25 | | | |
| Magnetite | 1.46 | 0.88 | 4.34 | 1.91 | 4.91 | 1.92 | 1.96 | 2.45 | 1.22 | 4.13 | 1.03 | 5.19 | 2.94 | | | |
| Hematite | – | – | – | – | 0.45 | – | – | – | – | – | – | 0.65 | 0.62 | | | |
| Ilmenite | 0.54 | 0.52 | 0.66 | 0.81 | 0.73 | 1.13 | 1.03 | 0.74 | 1.19 | 0.82 | 0.84 | 0.75 | 0.69 | | | |
| Apatite | 0.11 | 0.11 | 0.11 | 0.11 | 0.11 | 0.11 | 0.11 | 0.11 | 0.11 | 0.11 | 0.11 | 0.11 | 0.11 | | | |
| Col. Index | 5.58 | 5.53 | 7.6 | 7.11 | 6.59 | 11.11 | 4.71 | 5.07 | 6.18 | 6.99 | 5.79 | 7.09 | 4.5 | | | |
| Diff. Index | 91.34 | 91.14 | 92.12 | 90.38 | 91.06 | 80.94 | 86.84 | 91.85 | 87.68 | 90.35 | 87.38 | 92.37 | 93.48 | | | |
| Sample | CL-74 | CL-87 | GA-68 | JP-49 | JP-50 | PPB-14 | PPB-14a | CL-77 | CL-88 | GA-13 | GA-14 | GA-14b | PPB-28a | PPB-63 | PPB-64 | CL-09 |
| Quartz | 25.43 | 33.5 | 31.19 | 18.68 | 33.61 | 26.72 | 21.18 | 36.81 | 33.11 | 39.62 | 26.32 | 23.21 | 29.68 | 10.27 | 31.14 | 24.51 |
| Corundum | – | – | – | – | – | – | – | 1.79 | – | 0.65 | – | – | – | – | 1.26 | – |
| Orthoclase | 30.36 | 27.43 | 29.85 | 30.41 | 29.15 | 29.74 | 29.92 | 39.9 | 29.32 | 29.23 | 26.37 | 24.5 | 33.36 | 25.3 | 29.76 | 29.86 |
| Albite | 35.63 | 31.23 | 32.48 | 40.87 | 28.96 | 34.08 | 41.12 | 15.35 | 31.7 | 22.21 | 34.33 | 40.22 | 30.71 | 51.64 | 31.54 | 35.92 |
| Anorthite | – | – | 1.19 | – | 2.47 | – | 0.52 | 0.02 | 1.95 | 1.57 | 2.36 | 2.83 | 1.13 | – | 1.77 | 2.41 |
| Acmite | 2.41 | 1.82 | – | 2.36 | – | 2.99 | – | – | – | – | – | – | – | 0.1 | – | – |
| ns | – | – | – | – | – | – | – | – | – | – | – | – | – | – | – | – |
| Diopside | 2.56 | – | 2.14 | – | 0.04 | – | 3.15 | – | 0.95 | – | 2.85 | 2.08 | 1.88 | – | – | 0.95 |
| Hypersthene | 0.93 | 0.3 | 1.79 | 0.35 | 3.17 | 0.32 | – | 0.42 | 1.8 | 0.5 | 3.69 | 2.82 | 1.46 | 0.81 | 1.77 | 5.24 |
| Magnrtite | 2.15 | 4.48 | 0.94 | 5.09 | 2.04 | 4.19 | 4.55 | 4.3 | 0.85 | 4.91 | 2.79 | 3.23 | 1.34 | 5.82 | 2.19 | 0.54 |
| Hematite | – | 0.01 | – | 0.02 | – | 0.3 | – | 0.26 | – | 0.45 | – | – | – | 3.6 | – | – |
| Ilmenite | 0.4 | 0.71 | 0.29 | 0.84 | 0.42 | 0.82 | 0.42 | 1.01 | 0.19 | 0.73 | 1.12 | 0.98 | 0.31 | 0.77 | 0.44 | 0.44 |
| Apatite | 0.11 | 0.11 | 0.11 | 0.11 | 0.11 | 0.11 | 0.11 | 0.11 | 0.11 | 0.11 | 0.13 | 0.11 | 0.11 | 0.11 | 0.11 | 0.11 |
| Col. Index | 6.04 | 5.5 | 5.16 | 6.3 | 5.68 | 5.64 | 7.13 | 6 | 3.79 | 6.59 | 10.45 | 9.1 | 4.98 | 11 | 4.4 | 7.17 |
| Diff. Index | 91.42 | 92.16 | 93.52 | 89.97 | 91.73 | 90.53 | 92.22 | 92.06 | 94.13 | 91.06 | 87.03 | 87.94 | 93.75 | 87.2 | 92.44 | 90.29 |

Transamazonian event. The COIS is a typical example of a late-Transamazonian suite, Ca- and Al-richer than the SMS, and according to the genetic scheme suggested by Bonin (1982), these granites are earlier than the peralkaline types. The SMS has composition very similar to anorogenic suites. The strong deformation caused by continental collision during the Brasiliano event, as well as the Transamazonian age of carbonatitic rocks in this region, suggest that the SMS is related to continental rift setting after the Transamazonian event.

## Acknowledgements

This work was supported by CNPq and CAPES. J.P.C. thanks to Professor Jean-Michel Lafon for isotopic determinations on the Couro-de-Onça and Serra do Meio Suits, accomplished at the Geochronological Laboratory from Federal University of Pará, Brazil; the Fundação Coordenação de Aperfeiçoamento de Pessoal de Nível Superior (CAPES-no. 1772/95-14), the Centro de Estudos em Petrologia e Geoquímica-UFRGS, Programa de Pesquisa e Pós-Graduação em Geofísica, PPPG-UFBA, Département des Sciences de la Terre, Centre d'Orsay, Université de Paris-Sud, and his wife, for her patience.

## References

Almeida, F.F.M., Hasui, Y., Brito Neves, B.B., 1977. Províncias Estruturais Brasileiras. Simp. Geol. Nord., Campina Grande-PB, Anais, pp. 363–391.

Ashley, P.M., Cook, N.D.J., Fanning, C.M., 1996. Geochemistry and age of metamorphosed felsic igneous rocks with A-type affinities in the Willyama supergroup, Olary Block, South Australia, and implications for mineral exploration. Lithos 38, 167–184.

Barbosa, J.S.F., Dominguez, J.M.L., 1996. Mapa geológico do Estado da Bahia. Texto Explicativo. Secretaria da Indústria, Comércio e Mineração do Estado da Bahia. PPPG-UFBA, Salvador, Brasil.

Bonin, B., 1980. Le complexes acides alcalins anorogéniques continentaux: l'exemple de la Corse. Doct. Etat ès-Sci. Thesis, Université Pierre et Marie Curie, Paris, France.

Bonin, B., 1982. Les granites des complexes annulaires. B.R.G.M. (Ed.) Manuels et Méthodes no. 4, Orléans, p. 147.

Bonin, B., 1987. From orogenic to anorogenic magmatism: a petrological model for the transition calk-alkaline–alkaline complexes. Internatinal Symposium on Granites and Association of Mineral. Salvador, Brazil, Extended Abstracts, pp. 27–31.

Bonin, B., 1988. Peralkaline granites in Corsica: some petrological and geochemical constraints. Rend. Della Soc. Ital. Miner. Petrol. 43 (2), 281–306.

Bowden, P., Turner, D.C., 1974. Peralkaline and associated ring-complexes in the Nigeria — Niger province, west Africa. In: Sorensen, H. (Ed.), The Alkaline Rocks. Wiley, London, pp. 330–351.

Bowden, P., Whitley, J.E., 1974. Rare-earth patterns in peralkaline and associated granites. Lithos 7, 15–21.

Bowden, P., Kinnaird, J.A., 1978. Younger granites of Nigeria — a zinc-rich tin province. Trans. Sec. B Inst. Miner. Met. 87, 66–69.

Bowden, P., Kinnaird, J.A., 1984. The petrology and geochemistry of alkaline granites from Nigeria. Phys. Earth Planet Int. 35, 199–211.

Brito Neves, B.B., 1975. Regionalização geotectônica do Pré-Cambriano nordestino. Tese de Doutorado, Instituto de Geociências, Universidade de São Paulo, Brasil.

Charoy, B., Raimbault, L., 1994. Zr-, Th-, and REE-rich biotite differentiates in the A-type granite pluton of Suzhou (Eastern China): the key role of fluorine. J. Petrol. 35 (4), 919–962.

Collins, W.J., Beams, S.D., White, A.J.R., Chappell, B.W., 1982. Nature and origin of A-type granites with special reference to southeastern Australia. Contrib. Miner. Petrol. 80, 189–200.

Conceição, H., 1990. Pétrologie du massif syénitique d'Itiúba: contribution à l'étude minéralogique des roches alcalines dans l'Etat de Bahia (Brésil). Tese de Doutorado, Université Paris-Sud, Centre d'Orsay, France.

Conceição, R.V., 1994. Petrologia dos sienitos potássicos do maciço de Santanapólis e alguns aspectos do seu embasamento granulítico. Dissertação de Mestrado, CPGG-UFBA, Salvador, Brasil.

Couto, L.F., 1989. Estudo petrológico do complexo máfico-ultramáfico de Campo Alegre de Lourdes e dos óxidos de Fe, Ti, (V) associados. Dissertação Mestrado, Universidade de Brasília-UNB, Brasília, Brasil.

Czamanske, G.K., Dillet, B., 1988. Alkali amphibole, tetrasilicic mica, and sodic pyroxene in peralkaline siliceous rocks, Quest caldera, New Mexico. Am. J. Sci. 288-A, 358–392.

Dall'Agnol, R., Lafon, J.-M., Macambira, M.J.B., 1994. Proterozoic anorogenic magmatism in the central Amazonian province, Amazonian craton: geochronological, petrological and geochemical aspects. Miner. Petrol. 50, 113–138.

Dalton de Souza, J.A., Fernandes, F.J., Guimarães, J.T., Lopes, J.N., 1979. Projeto colomi: geologia da região do Médio São Francisco. Relatório final, DNPM/CPRM, Salvador, Brasil.

Don Hermes, O., Zartman, R.E., 1992. Late proterozoic and silurian alkaline plutons within the southeastern New England Avalon zone. J. Geol. 100 (4), 477–486.

Dooley, D.F., Patiño Douce, A.E., 1996. Fluid-absent melting of F-rich phlogopite + rutile + quartz. Am. Miner. 81, 202–212.

Ernst, W.G., 1962. Synthesis, stability relations, and occurrence of riebeckite and riebeckite-arfvedsonite solid solutions. J. Geol. 70, 689–736.

Evensen, N.M., Hamilton, P.J., O'Nions, R.K., 1978. Rare earth abundances in chondritic meteorites. Geochim. Cosmochim. Acta 42, 1199–1212.

Ferreira, V.P., Sial, A.N., Whitney, J.A., 1994. Large scale silicate immiscibility: a possible example from northeast Brazil. Lithos 33, 285–302.

Figuerôa, I., Silva Filho, I., 1990. Geologia da Folha Petrolina. In: Prog. Levant. Geol. Bás. do Brasil (PLGBB) Folha SC.24-V-C-III Petrolina. DNPM/CPRM, Rio de Janeiro, pp. 11–56.

Gastal, M.C.P., Nardi, L.V.S., 1992. Petrogênese e Evolução do Granito Jaguari: um típico representante metaluminoso da Suíte Intrusiva Saibro, RS. Geochem. Brasil 6 (2), 169–189.

Harris, N.B.W., 1980. The role of fluorine and chlorine in the petrogenesis of a peralkaline complex from Saudi Arabia. Chem. Geol. 31, 303–310.

Hibbard, M.S., 1995. Petrography to Petrogenesis. Prentice-Hall, Englewood Cliffs, NJ.

Jacobson, R.R.E., Mac Leod, W.N., Black, R., 1958. Ring-complexes in the Younger granite province of northern Nigeria. Geol. Soc. London Mem. 1, 1–72.

Jardim de Sá, E.F., 1994. A faixa Seridó (Província Borborema, NE do Brasil) e o seu significado geodinâmico na cadeia Brasiliana/Pan-Africana. Tese de Doutorado, Universidade de Brasília, Brasil.

Leite, C.M., 1987. Projeto Remanso II. Relatório Final. CBPM-SME, Salvador, Brasil.

Leite, C.M., 1993. Caracterização dos maciços alcalinos como granitos tipo-A na Província Toleítica Alcalina de Campo Alegre de Lourdes (Bahia). IV Cong. Bras. Geoq., São Paulo, SP, Bol. Res. Exp., pp. 38–40.

Leite, C.M., 1997. Programa de Levantamentos Geológicos Básicos do Brasil, Folha-SC.23-X-D-IV (Campo Alegre de Lourdes), escala 1Ê:100000. CBPM/CPRM/SICM, Salvador, Brasil.

Leite, C.M., Fróes, R.J.B., 1989. Características petroquímicas do granito alcalino Serra do Meio (Campo Alegre de Lourdes-Estado da Bahia). II Cong. Bras. Geoq., Rio de Janeiro-RJ, Anais, 1, pp. 157–167.

Leite, C.M., Conceição, H., Cruz, M.J., 1991. Plutonismo hiperalcalino supersaturado da Província de Campo Alegre de Lourdes: evolução mineraloquímica e suas implicações. III Cong. Bras. Geoq., São Paulo, Anais, 2, pp. 717–721.

Leite, C.M.M., Santos, R.A., Conceição, H., 1993. A província toleiítica-alcalina de Campo Alegre de Lourdes: geologia e evolução tectônica. II Simpósio sobre o Cráton do São Francisco. SBG/SGM, Salvador-Brasil, Anais, 1, pp. 56–59.

Le Maitre, R.W., Bateman, P., Dubek, A., Keller, J., Lameyre, J., Le Bas, M.J., Sabine, P.A., Schimid, R., Sorensen, H., Streckeisen, A., Wooley, A.R., Zanettin, B. (Eds.), 1989. A Classification of Igneous Rocks and Glossary of Terms: Recommendations of the International Union of Geological Sciences Subcommission on the Systematics of Igneous Rocks. Blackwell (Basil), Oxford.

Luth, W.C., Tuttle, O.F., 1966. The alkali-feldspar solvus in the system $Na_2O$–$K_2O$–$Al_2O_3$–$SiO$–$H_2O$. Am. Miner. 51 (9/10), 1359–1373.

Mahood, G., Hildreth, W., 1983. Large partition coefficients for trace elements in high-silica rhyolites. Geochim. Cosmochim. Acta 47 (1), 11–30.

Maniar, P.D., Piccoli, P.M., 1989. Tectonic discrimination of granitoids. Geol. Soc. Am. Bull. 101, 635–643.

Middlemost, E.A.K., 1994. Naming materials in the magma/igneous rock system. Earth Sci. Rev. 37, 215–224.

Miller, C.F., Mittlefehldt, D.W., 1984. Extreme fractionation in felsic magma chambers: a product of liquid-state diffusion or fractional crystallization? Earth Plan. Sci. Lett. 68 (1), 151–158.

Nardi, L.V.S., 1991. Caracterização petrográfica e geoquímica dos granitos metaluminosos da associação alcalina: revisão. Pesquisas 18 (1), 44–57.

Nardi, L.V.S., Bonin, B., 1991. Post-orogenic and non-orogenic alkaline granite associations: the Saibro intrusive suite, southern Brazil — a case study. Chem. Geol. 92, 197–212.

Neksvasil, H., 1992. Ternary feldspar crystallization in high-temperature felsic magmas. Am. Miner. 75 (5/6), 592–604.

Patiño Douce, A.E., Beard, J.S., 1996. Effects of P, f($O_2$)and Mg/Fe ratio on dehydration melting of model metagreywackes. J. Petrol. 37 (5), 999–1024.

Pearce, J.A., Norry, M.J., 1979. Petrogenetic implications of Ti, Zr, Y e Nb variation in volcanic rocks. Contrib. Miner. Petrol. 69, 33–47.

Pearce, J.A., Harris, N.B.W., Tindle, A.G., 1984. Trace element discrimination diagrams for the tectonic interpretation of granitic rocks. J. Petrol. 25, 956–983.

Plá Cid, J., 1994. Granitogênese alcalina de Campo Alegre de Lourdes (Norte da Bahia): Petrografia, Mineraloquímica e Geoquímica. Dissertação de Mestrado, CPGG-UFBA, Salvador, Brasil.

Plá Cid, J., Conceição, H., Nardi, L.V.S., 1995. As micas tri-octaédricas da suíte granítica de Campo Alegre de Lourdes (N da Bahia). V Cong. Bras. Geoq. and III Cong. Geoq. dos Países de Língua Port., CD-Rom, Niterói-Brasil.

Plá Cid, J., Nardi, L.V.S., Conceição, H., Bonin, B., 1997a. O magmatismo alcalino da faixa de dobramentos Riacho do Pontal e da borda noroeste do Cráton do São Francisco, norte do Estado da Bahia, Brasil: uma síntese. X Semana de Geoq. e IV Cong. Geoq. dos Países de Língua Portuguesa, Braga, Portugal, Actas., pp. 127–130.

Plá Cid, J., Nardi, L.V.S., Conceição, H., Bonin, B., 1997b. Alkalic plutonic activity within in the Riacho do Pontal

fold belt, NE Brazil. Second ISGAM, Ext. Abst. and Prog., Salvador-Brasil, pp. 143–144.

Rosa, M.L.S., 1994. Magmatismo shoshonítico e ultrapotássico no sul do cinturão móvel Salvador-Curaçá, maciço de São Félix: Geologia, mineralogia a geoquímica. Dissertação de mestrado, CPGG-UFBA, Salvador, Brasil.

Scogings, A.J., 1986. Trans. Geol. Soc. South Afr. 89, 361–365.

Silva, M.E., 1987. O sistema de dobramentos Rio Preto e suas relações com o Cráton do São Francisco. Dissertação de Mestrado, Instituto de Geociências, Universidade de Brasília, Brasil.

Silva, A.B., Liberal, G.S., Grossi Sad, J.M., Issa Filho, A., Rodrigues, C.S., Riffel, D.F., 1988. Geologia e petrologia do complexo Angico dos Dias (Bahia, Brasil), uma associação carbonatítica précambriana. Geochem. Bras. 2 (1), 81–108.

Sorensen, H., 1974. The Alkaline Rocks. Wiley, London.

Thirwall, M.F., Jones, N.W., 1983. Isotope geochemistry and contamination mechanics of tertiary lavas from Skye, Northwest Scotland. In: Hawkesworth, C.J., Norry, M.J. (Eds.), Continental Basalts and Mantle Xenoliths. Shiva, Nantwich, pp. 186–208.

Van Schmus, W.R., Brito Neves, B.B.D., Hackpacher, P., Babinski, M., 1995. U–Pb and Sm–Nd geochrnologic studies on eastern Borborema province, northeastern Brazil: initial conclusions. J. South Am. Earth Sci. 8 (3/4), 267–288.

Watson, E.B., 1979. Zircon saturation in felsic liquids: experimental results and applications to trace element geochemistry. Contrib. Miner. Petrol. 70, 407–419.

Watson, E.B., Harrison, T.M., 1983. Zircon saturation revisited: temperature and composition effects in a veriety of crustal magma types. Earth Plan. Sci. Lett. 64, 295–304.

Wernick, E., 1981. The Archean of Brazil. Earth Sci. Rev. 17, 31–48.

Whalen, J.B., Currie, K.L., Chappell, B.W., 1987. A-type granites: geochemical characteristics, discrimination and petrogenesis. Contrib. Miner. Petrol. 95, 407–419.

Wilson, M., 1989. Igneous Petrogenesis: A Global Tectonic Approach. Unwin Hyman, London, UK.

Winkler, H.G.F., 1979. In: Winckler, H.G.F. (Ed.), Petrogenesis of Metamorphic Rocks. Springer, New York.